



THE UNIVERSITY OF QUEENSLAND  
A U S T R A L I A

# Distributed parameter modelling of phototrophic systems

Edward Barry

B.Eng. (Hons)

*A thesis submitted for the degree of Doctor of Philosophy at  
The University of Queensland in 2018*

School of Chemical Engineering

# Abstract

Purple phototrophic bacteria (PPB) are known to exist in a variety of environments and have been demonstrated as a potentially effective biotechnology in several industries such as wastewater treatment, cosmetics production, and energy production. Although PPB processes are gaining relevance in the aforementioned industries, physical limitations exist which are providing resistance to the widespread adoption of PPB based biotechnology. This thesis has aimed to define the most important limitations and has sought to define their physical behaviour in a mathematical framework. The first limitation was that there was no PPB process model describing the behaviour of PPB in the presence of ammonia, organic matter, and other nutrients. The mixed population models of the International Water Association (IWA) family of models describe species whose metabolism differ from that of PPB but they provide a good framework for process modelling and control. As such, a process model for a mixed-culture PPB system was developed based on five key processes: photoheterotrophic growth, photoautotrophic growth, chemoheterotrophic growth, hydrolysis/fermentation, and decay. This model was developed as a set of ordinary differential equations varying in time, and lumped in space. The sharp attenuation of the radiative field in a PPB system means that not all the biomass experiences the same radiative field in a reactive domain. This means that the model required an extension to be able to describe the system as it varies in both space and time. A CFD modelling framework was therefore developed in OpenFOAM to describe the spatial variations and interactions between biomass growth, the flow field, and the radiative field. It was found that lumped modelling approaches and distributed parameter approaches differed in results based on different reactor domains and behaviours. The deviation from lumped parameter behaviour was greater for a cylindrical stirred reactor than for a flat plate reactor, which means that spatial considerations are necessary in the design phase of a photobioreactor. Finally, technical questions around the harvesting of PPB biomass present significant engineering challenges and are a limitation to the adoption of this biotechnology. The model was thus extended to include biofilm formation of a mixed PPB system in the presence of a spatially varying radiative field. A volume-of-fluid approach was used as a basis for this model, where particulate matter was segregated to the phase volume fraction, and the growth of the three particulate species (phototrophic bacteria, biodegradable particulate matter, and inert particulates) were included as source terms to the phase volume fraction equations, which in turn influenced the momentum equations, resulting in biofilm growth in space.

The combination of all of these methods provide a working PPB modelling framework which can form the basis to better understand PPB (and phototrophic) systems within a process modelling context, and with further experimental analysis, can provide a foundation for a photobioreactor design and optimisation project.

## **Declaration by author**

This thesis is composed of my original work, and contains no material previously published or written by another person except where due reference has been made in the text. I have clearly stated the contribution by others to jointly-authored works that I have included in my thesis.

I have clearly stated the contribution of others to my thesis as a whole, including statistical assistance, survey design, data analysis, significant technical procedures, professional editorial advice, financial support and any other original research work used or reported in my thesis. The content of my thesis is the result of work I have carried out since the commencement of my higher degree by research candidature and does not include a substantial part of work that has been submitted to qualify for the award of any other degree or diploma in any university or other tertiary institution. I have clearly stated which parts of my thesis, if any, have been submitted to qualify for another award.

I acknowledge that an electronic copy of my thesis must be lodged with the University Library and, subject to the policy and procedures of The University of Queensland, the thesis be made available for research and study in accordance with the Copyright Act 1968 unless a period of embargo has been approved by the Dean of the Graduate School.

I acknowledge that copyright of all material contained in my thesis resides with the copyright holder(s) of that material. Where appropriate I have obtained copyright permission from the copyright holder to reproduce material in this thesis and have sought permission from co-authors for any jointly authored works included in the thesis.

## **Publications included in this thesis**

### **Submitted manuscripts included in this thesis**

### **Other publications during candidature**

#### **Conference abstracts**

#### **Book chapters**

### **Contributions by others to the thesis**

My advisory team of Prof. Damien Batstone, A/Prof. Christopher DeGroot, and Dr. Tim Hülsen provided feedback on the work presented. A/Prof. Christopher DeGroot contributed to some development at the early stages of the research project, and was instrumental in help with debugging as a set of fresh eyes towards the end of the research project.

### **Statement of parts of the thesis submitted to qualify for the award of another degree**

No works submitted towards another degree have been included in this thesis.

### **Research involving human or animal subjects**

No animal or human subjects were involved in this research.

## **Acknowledgments**

## **Financial support**

### **Keywords**

Computational fluid dynamics, purple phototrophic bacteria, process modelling, mechanistic modelling, biofilms,

### **Australian and New Zealand Standard Research Classifications (ANZSRC)**

ANZSRC code: 091501, Computational Fluid Dynamics, 50%

ANZSRC code: 090702, Environmental Engineering Modelling, 40%

ANZSRC code: 090409, Wastewater Treatment Processes, 10%

### **Fields of Research (FoR) Classification**

FoR code: 0915, Interdisciplinary Engineering, 50%

FoR code: 0907, Environmental Engineering, 40%

FoR code: 0904, Chemical Engineering, 10%

---

# Contents

---

Abstract . . . . .	ii
<b>Contents</b>	vii
<b>List of figures</b>	ix
<b>List of tables</b>	x
<b>List of abbreviations and symbols</b>	xi
<b>1 Introduction</b>	1
1.1 Motivation . . . . .	1
1.2 Background . . . . .	2
1.2.1 Time varying wastewater treatment models . . . . .	2
1.2.2 Computational fluid dynamics for wastewater treatment and photobioreactors	4
1.2.3 Radiation Modelling . . . . .	8
1.2.4 Biochemical Equations Modelling . . . . .	12
1.2.5 Coupling of Physical Processes . . . . .	13
1.3 Research objectives and approach . . . . .	14
1.3.1 Research objective 1: A description of the process biokinetics of phototrophic systems . . . . .	15
1.3.2 Research objective 2: . . . . .	15
<b>2 A description of the process biokinetics of phototrophic systems</b>	17
2.1 Introduction . . . . .	17
<b>3 Computational fluid dynamics analysis of single and two-phase photobioreactors</b>	19
3.1 Introduction . . . . .	19
3.2 Methods . . . . .	22
3.2.1 Geometry and mesh generation . . . . .	22
3.2.2 Fluid flow . . . . .	23
3.2.3 Radiative transport . . . . .	25
3.2.4 Biokinetic model . . . . .	28

3.2.5	Solution procedure . . . . .	28
3.3	Results and Discussion . . . . .	30
3.3.1	Radiative field dynamics . . . . .	30
3.3.2	Short-term particle radiation dynamics . . . . .	30
3.3.3	Growth of PPB biomass and uptake of soluble substrates . . . . .	32
3.3.4	Limitations of the model . . . . .	35
3.4	Conclusions . . . . .	36
<b>4</b>	<b>A multidimensional, phototrophic, continuum biofilm model</b>	<b>39</b>
4.1	Introduction . . . . .	39
4.1.1	Processes governing the biofilm lifecycle . . . . .	39
4.1.2	Examples of beneficial and harmful biofilms . . . . .	40
4.1.3	Modelling of photobiofilms . . . . .	40
4.2	Problem description . . . . .	45
4.3	Mathematical formulation . . . . .	46
4.3.1	Radiative transfer . . . . .	46
4.3.2	Consumption and release of soluble substrates . . . . .	46
4.3.3	Growth of particulate matter . . . . .	47
4.3.4	Pressure term . . . . .	47
4.3.5	Boundary and initial conditions . . . . .	47
4.4	Numerical Treatment . . . . .	47
4.5	Implementation . . . . .	47
4.6	Discussion . . . . .	47
4.7	Conclusions . . . . .	47
<b>5</b>	<b>Conclusions and outlook</b>	<b>49</b>
<b>Bibliography</b>		<b>51</b>

---

# List of figures

---

3.1	Representation of the geometries of the FPR (a) and the CR (b) upon which the simulations were based. The depth of the FPR is 6.0 cm. The blue region of the FPR represents the initial liquid volume fraction in the reactor, with the grey region representing the headspace. A single liquid phase was simulated in the case of the CR. . . . .	22
3.2	Solution algorithm for the solver. Momentum equations are solved until steady state is achieved and fed to the biochemical equation solver. The radiative field is updated every 15 minutes of simulated time. . . . .	29
3.3	Evolution of the radiative field ( $\text{Wm}^{-2}$ ), volume averaged over all time steps, and the spatial changes over time for the FPR and CR. Cross-sectional view at reactor from 0 cm to 3 cm from the radiation source. (b,c) corresponds to the radiative field at the start of the simulation, and (d,e) is the radiative field at 24 hours for the FPR and CR respectively. . . . .	31
3.4	Particle radiation dynamics for an 850 nm band of irradiance. The top row (a, b) shows the transient radiative field experienced by a PPB particle for the FPR and CR reactors respectively. The same field is represented for both reactors (c, d) as a histogram on the bottom row. Both reactors have an incident irradiance of $30 \text{ Wm}^{-2}$ . . . . .	32
3.5	Biomass growth and substrate uptake for the FPR (a, c, e) and the CR (b, d, f). The first row shows the growth of PPB and the second and third rows show the consumption of acetic acid and other readily biodegradable soluble organics respectively. For all figures, the triangles correspond to ODE1, the diamonds correspond to ODE2, the crosses represent ODE3, and the solid line is the CFD solution. . . . .	34
4.1	Two-dimensional representation of the simulation domain for the case of a bottom-irradiated biofilm. Boundaries $\Gamma_4$ and $\Gamma_5$ are out of, and into the page respectively, and take the same boundary conditions as boundaries $\Gamma_1$ and $\Gamma_2$ . The irradiance source ( $h\nu$ ) is in fact uniform and diffuse across the whole boundary. Subscripts relating to $\alpha$ , namely <b>I</b> and <b>B</b> correspond to liquid phase fraction, and biofilm phase fraction respectively.	45

---

# List of tables

---

1.1	Maximum theoretical <i>Rb. capsulatus</i> yield with acetate as electron donor for different wavelengths [1] . . . . .	3
1.2	PPB experimental yield for different wavelengths and lactate and acetate as electron donors [1] . . . . .	4
3.1	FvDOM and biomass coupling parameters for the radiation component of the solution procedure . . . . .	27

---

# List of abbreviations and symbols

---

Abbreviations	
ADMn	Anaerobic digestion model (nth release)
ASMn	Activated sludge model (nth release)
CFD	Computational fluid dynamics
COD	Chemical oxygen demand
CR	Cylindrical reactor
DOM	Discrete ordinates method
FPR	Flat plate reactor
FvDOM	Finite volume discrete ordinates method
FVM	Finite volume method
HG	Henyey-Greenstein phase function
HPC	High performance computing
IWA	International Water Association
LH $n$	Light harvesting apparatus $n$ ; $n \in \{1, 2\}$
MC	Monte Carlo
NIR	Near-infrared radiation
ODE	Ordinary differential equation
PAR	Photosynthetically active radiation
PBR	Photobioreactor
PDE	Partial differential equation
PPB	Purple phototrophic bacteria
PSU	Photosynthetic unit
RANS	Reynolds-averaged Navier-Stokes
RC	Reaction centre
RPM	Revolutions per minute
RTE	Radiative transfer equation
SM	Schlick model
SST	Shear stress transport
TPF	Truncated phase function

---

Symbols	
$\hat{\rho}$	Density operator
<i>etc.</i>	<i>etc.</i>

---

# Chapter 1

---

## Introduction

---

### 1.1 Motivation

Purple phototrophic bacteria (PPB) have recently been proposed as an effective biotechnology for engineered applications including the treatment of domestic [2] and industrial wastewaters [3]. Phototrophic bacteria, along with their chromophores, have also shown promise in a range of highly valued end products such as animal feeds [4], biofuels [5], and even cosmetic and pharmaceutical products [6, 7]. Despite the increasing interest in these applications, they have not achieved widespread implementation largely due to the gaps in collective knowledge at the process level. In particular, the description and quantification of the interactions between biochemical behaviour, irradiation, and fluid hydrodynamics have proven to be significant design bottlenecks when scaling up photobioreactors.

By approaching the problem with a semi-mechanistic modelling approach, one can better understand these interactions and how their behaviour can influence the design and optimisation decisions at scale up. As such, this thesis aims to explore the current state of process modelling, computational fluid dynamics, and radiative transfer modelling and combine these concepts into a unified distributed parameter modelling framework for phototrophic systems and photobioreactors. Additionally, a deterministic, semi-mechanistic biofilm model is developed which draws upon the physical phenomena identified is also developed in response to the need to find a solution to engineering challenges associated with biomass harvesting.

## 1.2 Background

### 1.2.1 Time varying wastewater treatment models

Models use mathematical expressions to explain the underlying processes or inputs of outputs of a system [8]. They can be classed according to the method of their development. When developing process models, a number of decisions can be made depending on the nature of the model and the information required for understanding.

- Mechanistic or empirical models
- Continuous or discrete models
- Lumped parameter (well-mixed) or distributed parameter models
- Stochastic or deterministic models

In reality, a model can be made using a combination of these different categories, depending on the target use of the model. Most of the available literature for wastewater treatment models is concerned with semi-mechanistic, continuous, lumped parameter and deterministic approaches to modelling. The major generic models in the domain of wastewater treatment, from which this thesis branches, are the International Water Association (IWA) family of models. These include the activated sludge model family, and the anaerobic digestion model (ADM) [9] family. These have been combined together with appropriate unit process models such as clarifier models [10] into standardised plant-wide models **BSM**. Modelling of wastewater treatment processes can lead to a greater understanding of the underlying physics and biochemistry [11]. All IWA models are semi-mechanistic, which means that the model equations are based on known mechanistic phenomena, such as the presence of known biological clades, but the kinetic relationships are generally stochastic.

These models are useful in understanding the underlying biochemical processes occurring on wastewater treatment systems. They also serve as good tools for process unit design in wastewater treatment plants. The benefits of these models are that they are readily extensible, and allow themselves to be used in distributed parameter models [12]. This also means that the IWA models can be applied for PPB time-series and distributed parameter models in contexts broader than just wastewater treatment.

#### Purple phototrophic bacteria growth models

Purple phototrophic bacteria are some of the most metabolically versatile organisms on earth [13]. They have been shown to grow well as photoheterotrophs under anaerobic conditions [14]. They also grow chemoheterotrophically in the absence of irradiation, and they grow photoautotrophically using irradiance to drive CO<sub>2</sub> fixation [15]. With respect to the modelling of phototrophic bacteria, there currently exist no models in the context of wastewater treatment and industrial growth in mixed systems on nutrients and organics, however the suite of metabolic modelling of PPB is rich but not readily applicable for a process engineering perspective [16].

## Purple phototrophic bacteria and radiation modelling

PPB have evolved to efficiently harvest available solar radiation in aquatic environments [17]. Due to oxygenic photosynthetic organisms filtering radiation in the visible band in the upper aerobic zones of these aquatic systems, PPB have adapted to make use of remaining solar energy, which include green and near infra-red (NIR) radiation [17]. The light harvesting apparatus in *Rhodobacterales* consists of two light harvesting complexes (LH2 and LH1), and a reaction centre (RC) [18]. A useful abstraction of the light harvesting complex is two distinct zones (LH2 and an LH2-RC complex) with absorbance spectra at 800-850 nm and 880 nm respectively. Figure cite: figure demonstrates how these light harvesting centres are arranged and how they participate in providing energy to the electron transport chain to ultimately generate ATP for growth and other cell processes. **DRAW A LHC SCHEMA IN LODRAW.**

In terms of modelling PPB and their interactions with photons for industrial applications, very little has been done. Most studies focusing on photobioreactor design have been for hydrogen production applications. [5], identified all studies were performed using pure cultures of either *Rhodobacter sphaeroides* or *Rhodopseudomonas palustris*. Further limitations to these works were that particular wavelengths were not selected, with most opting for direct sunlight or white tungsten or halogen lamps as light sources. These approaches are problematic for a wastewater treatment application, as the use of broad spectrum light will lead to competition by other heterotrophic bacteria, and other phototrophic and photosynthetic organisms found in domestic wastewater such as algae and cyanobacteria.

Efforts were made to combine a mass balance approach to the photoheterotrophic efficiency of PPB [1]. In this work, theoretical and experimental yields of purple phototrophic bacteria were calculated based on different electron donors and light sources. The maximum theoretical yields based on acetate as an electron donor are summarised in Table 1.1, where  $Y_{X/LE}^m$  is the maximum biomass growth per light energy dose;

Table 1.1: Maximum theoretical *Rb. capsulatus* yield with acetate as electron donor for different wavelengths [1]

Wavelength	$Y_{X/LE}^m$ ( $\text{gVSS} \cdot \text{kJ}^{-1}$ )
860 nm	0.020
744 nm	0.017
522 nm	0.012

The theoretical model was then compared to experimental data, with the following values obtained through experiment. This information is presented in Table 1.2.

Table 1.2: PPB experimental yield for different wavelengths and lactate and acetate as electron donors [1]

Species	Wavelength	Electron donor	$Y_{X/LE} \text{ (gVSS} \cdot \text{kJ}^{-1}\text{)}$
<i>Rb. capsulatus</i>	860 nm	lactate	0.018 - 0.031
<i>Rb. sphaeroides</i>	White ( $\lambda = 744 \text{ nm}$ )	acetate	0.009 - 0.016
<i>Rb. capsulatus</i>	522 nm	lactate	0.006 - 0.013

The data of [1] serves as an effective basis for quantifying and understanding the interactions between biomass growth, maintenance and decay, and the irradiance required for optimal reactor performance.

**Operating parameters from Berberoglu and Pilon, and Murphy and Berberoglu and Hale and Querrey.**

### 1.2.2 Computational fluid dynamics for wastewater treatment and photobioreactors

Traditional design methods of wastewater treatment process units consist of load and mass based static analysis, and testing of dynamic behaviour based on key operating state variables [19]. Computational fluid dynamics (CFD) is a cost-effective method for scaling up process units and testing variations in operating parameters. This allows the design of equipment without needing physical prototypes [20]. CFD involves the spatiotemporal numerical analysis of transport equations and chemical reactions [21]. There have been many applications for CFD, including aerodynamic studies of aircraft, turbine analysis in power plants, environmental modelling of pollutants, and biomedical analysis of blood flows [22]. The major CFD studies in water treatment modelling have been conducted in the fields of algae growth, the inactivation of pathogens by ultraviolet radiation, and geometry and flow optimisation of conventional treatment plant units such as clarifiers, ponds and digesters. These areas of application have been chosen as a basis for literature review, due to photobioreactors operating with similar physical phenomena such as radiation delivery, multiphase fluid flows, and biochemical reactions [23].

#### Bubble Column Models

There are numerous studies looking at modelling bubble columns in a spatio-temporal manner. One of the early works in this field identified a need to consider a modelling technique incorporating spatio-temporal variations in order to minimise capital and operating costs during scale-up of general bubble column reactors [24]. In this study, the Navier-Stokes system of equations modelled the continuous fluid phase, and the dispersed gas bubbles were modelled as discrete tracked particles, with their position being solved over time. As this was a 1994 study, the computing power limited the model development to a two dimensional 60 x 200 grid of a  $0.75\text{m}^2$  reactor face. Numerical diffusion arose when both the liquid and gas were considered as continuous phases. With the improvement in desktop computing capacity, CFD has been used extensively for bubble column and airlift reactor validation

using both approaches [23]. Other studies have looked at describing bubble flow within different reactor geometries with Eulerian-Eulerian (both phases considered continuous) methods [25–30]. Gas-liquid flow in bubble columns has also been investigated with Eulerian-Lagrangian (continuous liquid phase and discrete gas phase) models [31]. The major works in this field have looked at different geometry bubble columns with drag force, virtual mass force, lift force primarily with two dimensional geometries [29, 32–36]. These studies looked at the sensitivity of the columns to such parameters and conditions as turbulence model, sparger location, superficial gas velocity, reactor aspect ratio and virtual mass.

### ***Limitations of Bubble Column Studies***

The main strength of these bubble column CFD models is that they are applied to general simple geometries, as the main focus was to isolate the bubble flows to explain the effects of the principal hydrodynamic operating conditions and parameters. These general approaches to CFD modelling of bubble columns present a strong platform from which to commence photobioreactor simulations, but they also lead to limitations in the context of purple phototrophic bacteria for wastewater treatment. Even if solids are present in the system being modelled, phases are modelled as liquid and gas. Modelling approaches for solid phases require refinement, in which the solids are modelled as discrete particles, and the liquid and gas phases are modelled as continuous phases. In addition, these cases used simple geometries, which will probably not be appropriate for photobioreactor modelling and design, as the irradiated surface to volume ratio plays an important role in reactor performance [37]. Another note is that the generality of these cases means that biochemical reactions and photon-biomass interactions were not included in the studies.

Phototrophic microorganisms pose promising solutions to current important technological challenges: the management of wastes such as atmospheric pollutants and wastewater, production of high value products from waste streams, such as biofuels and bio-plastics [2]. They are resilient under favourable radiative conditions, quickly out-competing other non photosynthetic organisms [38]. Photosynthetic and phototrophic microorganisms can be used in photobioreactors (PBR), which can be categorised based on whether the reactor is situated indoors or outdoors, its geometry (tubular, flat plate, raceway), whether it is anaerobic or aerobic, and the method of mixing (sparged, paddle wheel). The technology for these various applications has however not been widely adopted, partly due to gaps in understanding of good PBR design, and partly due to energy and utilities markets not being favourable to large scale implementations. A method to address the former is to undertake virtual prototyping using computational fluid dynamics CFD [23]. This allows rapid development and experimentation, without the traditional expenses incurred in the scale up process [39].

The use of CFD for PBR analysis has increased since the first few studies in the early 1980s [ ]. Wider access to commercial CFD software packages and suitable computational resources are likely factors in this uptake. Commercial packages allow the user to streamline the work flow from geometry design, to meshing, to case set up, to data analysis and visualisation. One must however be prudent when carrying out CFD studies of PBRs, because the automation and ease in setting up cases with

commercial packages could lead to undesirable or even non-validated and inaccurate solutions. Such issues of good CFD modelling practice and uncertainty quantification have been well documented in industries with a longer history of CFD usage [40–43]. More recently, efforts have been made to outline good CFD modelling practices in the context of wastewater treatment plants [44].

CFD modelling has aided in the understanding of hydrodynamic processes, and a comprehensive review was carried out in 2011 reflecting the status of CFD modelling of PBRs [23]. Most papers reviewed focused on the implications of certain geometry designs on flow characteristics. The papers were sampled to find a consensus on the use of a turbulence model. It was found that all studies reported used Reynolds-average Navier-Stokes (RANS) models, with the most popular being the standard  $k - \varepsilon$  model. The popularity of RANS models is not surprising, owing to their efficiency compared to more complex turbulence models. The ubiquitous use of the standard  $k - \varepsilon$  model is somewhat surprising, given the evidence which shows this model is quite poor in predicting separated flows [45]. Further, it is clear that improved  $k - \varepsilon$  models, such as the realizable  $k - \varepsilon$  model [46], as well as other improved RANS models, such as the  $k - \omega$  SST model [45, 47] have been developed to address such deficiencies.

The goal of this review is to not only provide an update in the state of the art CFD modelling practices, but to focus on the coupling and interactions between pertinent physical phenomena in PBR systems. Categories have been organised based on these physical processes, including hydrodynamics, radiation, biokinetics, porous media modelling for membrane and biofilm systems, and attempts to couple these processes. In addition, attention must be paid to analytical approaches including discretisation error evaluation. Guidelines from the Journal of Fluids Engineering can be adapted to this review [42].

This work is based the recommendations presented by [38], and will assess CFD for PBR based on the following performance indicators that were highlighted: mixing, “light” delivery, mass transfer (including  $CO_2$  delivery and  $O_2$  purging in the case of micro-algae), and total energy demand. The study also alluded to the necessity in understanding and using the interactions between mass and radiative transfer, physiology of the microorganism in question, and their radiation and substrate kinetics and dynamics. In addition to these components, we have also identified that biofilm formation is important, whether one wants to avoid it, or use it as a design feature [48].

- hydrodynamics, including mixing and mass transfer
- radiative transfer
- physiology and biokinetics
- biofilms
- methods for coupling all physical phenomena
- analysis of error and grid convergence

The solution for the flow of a fluid is obtained by numerical solution of the Navier-Stokes equations, along with addition models, as required, to account for multiple phases, turbulence, etc. Most often, the equations are discretised using a finite volume method (FVM), but can also be discretised using other methods such as the finite element, finite difference, or spectral methods. The most common CFD packages for PBR studies are ANSYS Fluent and ANSYS CFX, both of which are based on FVM. Although it has not been used extensively for CFD analysis of PBRs, OpenFOAM is another FVM-based CFD code which is open source.

### **Turbulence Modelling**

- RANS modelling
- Wall functions

### **Modelling of gas phases**

- DNS
- Eulerian
- VOF

### **Modelling of dispersed biosolid phases**

In general, there are two methodologies, Eulerian and Lagrangian, that can be implemented to solve the transport of a dispersed solid phase within continuous fluid phase(s) in a CFD simulation. The Eulerian approach treats the solid phase as a continuum and computes the concentration distribution based on the solution of a PDE that generally includes convective and diffusive terms, and may include various source and sink terms as required. The Lagrangian approach, on the other hand, involves the calculation of a large number of particle trajectories, based on Newton's second law, and models of all forces acting on the particles, such as drag, lift, and gravity. Each method has its own advantages and disadvantages, and, depending on the specific objectives of the study, one method may be more appropriate or efficient than the other. After outlining the details of each, recommendations will be made regarding the suitability of each for modelling PBR systems.

In the Eulerian modelling approach, the flow field and concentration distribution of the particulate phase are calculated in sequence. The PDE governing the particle phase concentration is [49] (add more references)

$$\frac{\partial C}{\partial t} + \nabla \cdot (\mathbf{u}C) = \Gamma \nabla^2 C + S_c \quad (1.1)$$

The second term on the left side of Eq. 1.1 represents convection of the particles with the velocity of the fluid phase(s), coupling the flow and concentration fields. This coupling is one-way since

the solids concentration does not influence the flow field. The first term on the right side of Eq. 1.1 represents diffusion, while the second term represents all sources and sinks.

Discuss diffusion coefficient

Discuss relative motion of solid wrt fluid and drift flux

Equation based on [49]; check other sources to ensure it's general.

$$\frac{d\mathbf{u}_p}{dt} = F_D(\mathbf{u} - \mathbf{u}_P) + g \frac{\rho_p - \rho}{\rho_p} + \mathbf{F}_a \quad (1.2)$$

### Comparison of Eulerian and Lagrangian Methodologies

The Eulerian and Lagrangian approaches have been compared previously for particle transport in enclosed air spaces [49] (others?). Here the comparison is considered specifically in the context of PBR systems.

### 1.2.3 Radiation Modelling

There are many approaches to modelling the radiation within photobioreactors, each with different levels of complexity and effectiveness. The general form of the radiative transfer equation for a participating medium, upon which the approximations are based, is as follows [50]:

$$\begin{aligned} \frac{dI_\lambda(\mathbf{r}, \mathbf{s})}{ds} &= \kappa_\lambda I_{b\lambda} - (\kappa_\lambda + \sigma_{\lambda,s}) I_\lambda(\mathbf{r}, \mathbf{s}) \\ &\quad + \frac{\sigma_{\lambda,s}}{4\pi} \int_{4\pi} I_\lambda(\mathbf{r}, \mathbf{s}') \Phi_\lambda(\mathbf{s}, \mathbf{s}') d\Omega' \end{aligned} \quad (1.3)$$

Where;

$I_\lambda(\vec{r}, \vec{s})$  is the spectral intensity of a radiative ray [ $W \cdot m^{-2}$ ].

$\vec{r}$  is a position vector [ $m$ ].

$\vec{s}\vec{s}'$  are the radiation path direction and scattering direction respectively.

$\kappa_\lambda$  is the spectral absorption coefficient [ $m^{-1}$ ].

$\sigma_{\lambda,s}$  is the scattering coefficient [ $m^{-1}$ ].

$s$  is the path length [ $m$ ].

$\Phi_\lambda$  is the spectral scattering phase function.

$\Omega'$  is the solid angle.

The left hand side of the equation is the rate of change of intensity along a direction, the first term on the right hand side is extinction (absorption and scattering) of the radiative intensity ray, and the second term on the right hand side is the gain due to in-scattering.

Usually black body emission can be omitted from the RTE, as the phenomenon of interest is the growth of biomass aided by absorption of photons. Flow rates and any external heat sources usually allow us to neglect this term [51].

### Beer-Lambert law

Among the most simple of radiative field solution techniques is the Beer Lambert law (equation 1.4).

$$\frac{I(x)}{I_0} = \exp(-\beta x) \quad (1.4)$$

This approach lumps the absorption ( $\kappa_\lambda$ ) and out-scattering ( $\sigma_\lambda$ ) coefficients into one extinction coefficient ( $\beta_\lambda$ ). The attenuation of radiation is modelled as a function of path length, concentration of the participating medium, and the extinction coefficient. The major problem with the Beer-Lambert law is that it neglects the effects of in-scattering, which can potentially give discrepancies of 20% in the final solution [52–54]. This can be translated to an assumption of isotropic scattering. The optical thickness in photobioreactors is much greater than unity, meaning that the assumption of isotropic scattering does not hold [50].

Where,  $I(x)$  is the irradiance at point  $x$ ,  $I_0$  is the incident irradiance. This equation can be adapted to a spectral equation by noting the dependence of the extinction coefficient on the wavelength. It is then a matter of integrating these spectral incident intensities into a total incident irradiance ( $G$ ) [53].

The process for designing photobioreactors with CFD has been to solve the fluid fields and then overlay the solution to the Beer-Lambert law. One can then gain insight into the radiation history of phototrophic particles, an important design parameter. [55] explored the effects of light attenuation and algal growth using a three dimensional Beer-Lambert law. The authors coupled the biomass growth to the radiation field as per the Eilers-Peeters model for photosynthetic biomass growth states as detailed in [56]. Wavelengths corresponding to pigment absorption were not considered, but the terms in the Eilers-Peeters model are adaptable to particular phototrophic organisms, which could be understood as an implicit treatment of spectral radiation. More on this study will be included in Section XXXX (coupled), as it is quite a comprehensive example of full photobioreactor modelling, incorporating particle transport, radiation delivery, and biomass growth. [57] also used the simple Beer-Lambert law to solve the radiative field within a PBR, on the way to solving more physics and focusing on the interactions involved between fluid flow, radiation, and growth kinetics. Other studies involving coupling also involved a similar approach [58].

There are many examples of studies looking at the *radiation history* of a phototrophic particle by solving the flow field and subsequently solving the radiative field. Particles are then introduced into the system, either as massless entrained particles, or as participating particles subjected to external forces [59]. The movement of these particles into and out of light and dark regions of the reactor can be analysed for insight into the growth characteristics induced by PBR design and operating condition variations. Some studies looked at the attenuation of light by algae and  $CO_2$  bubbles in a sparged bubble column PBR [60]. Other formations include raceway ponds [61, 62], and tubular photobioreactors with static mixers [63]. CFD was used to determine the light field of a hydrogen producing photobioreactor with *Rhodobacter sphaeroides* [64]. A cylindrical continuous stirred PBR was used as the test case. An empirical radiation expression was used in an attempt to better approximate the scattering processes within a reactor. The method was adapted from a previous study [65]. The following hyperbolic model with empirical attenuation parameters  $K_l$ ,  $K_c$  and  $\varepsilon_m$  relating to scattering due to the dry weight

concentration of biomass ( $c_{dw}$ ) and path length ( $l$ ), and the extinction due to maximal absorption ( $\varepsilon_m$ ) is:

$$\frac{I}{I_0}(c, l) = \exp \left[ \frac{\varepsilon_m l}{(K_c + c_{dw})(K_l + l)} \right] \quad (1.5)$$

This model holds under the assumption of monochromatic radiation. The purpose of this study was to carry out particle tracing simulations where the radiation history of the particle could be tracked over time with different impeller speeds. This allowed more control over interactions between photons and biomass, leading to a higher production of hydrogen with a lower impeller frequency. The simulations were not coupled to the biokinetics of the system. With the exception of [61, 64], there were no clear efforts to separate the extinction coefficient into its absorption and scattering components. More accurate solutions which account for biological photon absorption, out-scattering, as well as in-scattering exist. These solutions are more general, leading to more adaptability when exploring different reactor configurations **citations required**.

### Radiative transfer equation discretisation approaches

A potentially more accurate approach to determining the radiation field in a photobioreactor is to solve an approximation to the complete radiative transfer equation. Photons of particular frequency are absorbed by the pigments of phototrophic microorganisms [66]. It is therefore important to consider the spectral nature of the radiation in order to develop a deeper understanding of how the incident radiation is attenuated by either biomass absorption, or scattered by other components in the participating medium. There are several methods used to discretise the RTE, including the P-1 approximation, the discrete ordinates method (DOM), the finite volume discrete ordinates method (FVDOM), the Monte Carlo (MC) method, and the flux approximation [67]. Of this list of approaches, the DOM, FVDOM and MC methods allow for resolution of the total spectral radiative transfer equation on the existing mesh [68]. The best balance between computational effort and solution accuracy is the FVDOM [50, 68]. The FVDOM discretisation of the RTE shares a starting point with the DOM, with the angular discretisation being the point of difference. The direction of radiative intensity is allowed to vary within the solid angle for the FVDOM, whereas for the DOM does not allow for the radiative intensity to vary within the solid angle [69].

I will go through optical literature to see if there are better phase functions for moderately optically thick media (there are, the Schlick phase function gives very similar results to the HG phase function, but doesn't include the fractional exponent in the denominator, which can be very costly). This allows us to treat in scattering in Lorenz-Mie régime, without losing much information. This can be something to consider when dealing with PBR, especially when we involve the participation of gas bubbles, as they follow a completely different régime of scattering (Rayleigh scattering, not Lorenz-Mie).

The earliest instance of the application of the radiative transfer equation for a suspended solution of phototrophic organisms was carried out by [52]. In this study, Mie theory was used to determine anisotropic scattering due to gas bubbles and the photosynthetic organisms. The resolution of the

fluence rate in the reactor depended on the concentration of *A. variabilis* within the reactor, but growth expressions were not considered. Like many optical studies of PBRs, the authors concluded that the Beer-Lambert law was an inappropriate method to predict irradiance in the PBR. The Henyey-Greenstein (HG) and truncated phase function (TPF) were compared relative to Mie Theory, and the TPF proved more useful as back scattering was better approximated in situations with gas bubbles and bacteria. This work formed a good starting point for radiation transfer in PBR. They elucidated many of the important factors to consider when modelling radiation transfer in PBR systems.

The FVDOM has been used with varying degrees of complexity in subsequent PBR CFD papers. Many studies treat photosynthetically active radiation (PAR) as a lumped quantity, *i.e.*  $\lambda \sim \mathcal{U}(400\text{ nm}, 700\text{ nm})$  [37, 70–73].

As stated in [74], savings in calculation times can be made with astute choices in solution scheduling. If assumptions are made that the state of the participating media is constant for a certain period of time, radiation calculations can be carried out more sparsely than the flow field or the biomass growth components of the simulation. With the pigments of phototrophic biomass absorbing at particular wavelengths, it is important to consider a spectral solution when solving for the radiation field. Approaching the problem in such a manner allows us to simulate how the biomass interacts with the radiation field more accurately. This allows the the exploration biological process related to the function of pigments, and design more appropriate PBRs. Examples of where spectral simulations were carried out using the FVDOM or DOM methods present a more accurate picture of the functionality of PBRs. For example, [74], conducted simulations on RTE modelling for an algal photobioreactor, looking at consequences of the selection of certain multiphase models on the solution of the RTE. The spectral FVDOM model was also seen as important for the design and scale up of photobioreactors, and as such, an open source model has been developed around the OpenFOAM framework [68]. This study also identified the need to develop accurate boundary conditions based on spectral radiation modelling. This model was then used in a paper outlining a quasi-complete modelling approach to algal photobioreactors [75]. There weren't any discernible changes to how the RTE was solved, but the optical model was supported by an hydrodynamic model and a biomass growth model. As this was a complete solution, it will be discussed and compared in greater detail in Section 1.2.5.

[76–79].

### Monte Carlo method

The Monte Carlo method for spectral irradiance has been seldom used in PBR CFD modelling. The method is the most accurate approximation of the resolution of the RTE, but high computing power is required to achieve a proper solution [68]. A study for the design of PBR using the MC method has been undertaken, with results being validated against experimental data [80].

### Two Flux Model

[53, 81–83]

## Summary of Radiation Modelling

The major conclusions to be drawn from previous attempts at radiation transfer modelling for PBR is that a balance needs to be found between simplicity and accuracy. Many PBR CFD studies have been found to be lacking with appropriate modelling approaches to solving the RTE. There is strong evidence to suggest that one must take into account the effects of in-scattering [50, 68, 74, 75, 79, 80]. [80], stated that the threshold beyond which one must start to consider the effects of in-scattering is  $100 \text{ mgL}^{-1}$  dry weight of biomass.

Keeping in mind that one of the major process bottlenecks to PBR design is the delivery of radiation, and that computing power is becoming cheaper, the future of CFD PBR modelling must include attempts to solve the RTE, including the effects of in-scattering, biological participation (or absorption) and non-biological participation.

For studies where wall-clock time is an important factor, one must start looking at making simplifications in other areas. Inspiration can be drawn from the field of graphical rendering theory, where the physical characteristics of photon transport are maintained, but processing times are greatly reduced [84].

The probability distribution of wavelength has not been considered, and Fourier transforms might be required for lamp boundary conditions for an appropriate simulation of real incident radiation. This would greatly aid in energy balance calculations for economic feasibility of PBRs.

### 1.2.4 Biochemical Equations Modelling

An extensive review has already been undertaken looking at efforts to couple radiative transfer with biomass growth and substrate uptake [56]. The focus on this work was for the outdoor cultivation of algae. The concepts however can be adapted to the cultivation and growth of other biomass species for a wide range of PBR configurations. The review looked at three major approaches to the modelling of algal growth: Type I models consisted of solving biokinetic models based on an incident irradiance, or average internal fluence rate. These models proved to be quite limiting in their ability to provide insight into the operation of outdoor photobioreactors. Type II models aim to solve the radiative field using the Beer-Lambert law, and type III models looked at solving the *light history* of the photosynthetic particles.

Modelling of the biological response to fluence rate can be achieved with either discrete or continuous models. The Eilers and Peeters model [85], considers the photosynthetic unit interacting with photons to occupy one of three states. The biomass  $X = \{x_1, x_2, x_3\}$ , where the transition  $x_1 \xrightarrow{\alpha I} x_2$  corresponds to the sufficient capture of photons at the required frequency to initiate the phototrophic biochemical reactions. The transition  $x_2 \xrightarrow{\gamma} x_1$  corresponds to the change to the dark cycle reactions. When the photosynthetic particle receives excessive irradiance, a transition occurs from an excited state to a photoinhibited state ( $x_2 \xrightarrow{\beta I} x_3$ ). The transition from a photoinhibited state to the resting state ( $x_3 \xrightarrow{\delta} x_1$ ). Figure REFIGURENUMBER represents these processes schematically DRAW SOMETHING SIMILAR TO A PRECEDENCE DIAGRAM. Include the examples of where CFD

studies have been done with the biomass being represented as a three state system.

Considering the biomass as a single state, with growth processes acting upon it, is another method. This single state can be coupled to important states, and solved over the flow field. Examples of states to which the biomass can be coupled are nutrients, radiation as a substrate, and other non phototrophic microorganisms. This method is based on the IWA family of models for wastewater treatment (ADM1, ASMx). There have not been many examples of a single state of phototrophic biomass, based on the modelling approaches found in the IWA family of models. **Include some models nonetheless - Bechet mentions a few of these models in a non CFD framework.**

### 1.2.5 Coupling of Physical Processes

In recent years, the access to computer power has increased significantly due to a number of reasons. Firstly, with the introduction of cloud services, one is able to pay per core-hour for access high performance computing (HPC) infrastructure. Secondly, with the introduction of single processor boards which can easily be placed in arrays to carry out parallel computational tasks, the price per FLOPS is decreasing. This means that in the field of PBR modelling, one can develop models which encompass more of the physical phenomena, leading to greater insight into the workings of PBRs, therefore better prediction power. However, as the miniaturisation of transistors approaches its limit, one will need to search for other methods to continue improving on turn around times for CFD simulations while increasing the **complexity (in the sense of more physics)** of PBR solutions.

The early PSU models looked at simulating algal PBRs by considering an irradiative field varying in space, and the resolution of biokinetic equations were coupled to this field [86–89]. The treatment of fluid dynamics in these models was implicitly tied to the time constants of the biochemical reactions [89]. A more complete investigation involved the coupling of the two-flux photon approach with the Lagrangian determination of cell trajectories and biomass concentrations [81]

$$\frac{dI^+}{dt} = -E_aXI^+ - bE_SX(I^+ - I^-) \quad (1.6)$$

$$\frac{dI^-}{dt} = -E_aXI^- - bE_SX(I^+ - I^-) \quad (1.7)$$

As can be seen from Equations 1.6 and 1.7, the irradiance has a dependency on the biomass concentration within the PBR. This approach only works under the assumption that at each level of depth  $\delta z$ , the biomass concentration is uniform. A more rigorous approach to solving the RTE is required if that is not the case [81]. The authors then go on to develop the model by solving the Reynolds averaged Navier-Stokes equations, with a stochastic fluctuation term included. The solution of the Eulerian flow field was then used as a basis for the Lagrangian-radiation coupling. The algal concentrations were assumed to be low enough, with an overall density similar to that of water, such that they could be considered as passive tracers in the PBR. The paths of algal cells were tracked and the overall irradiance profile was solved for each point in  $z$ . It is with the history of the algal cells,

along with the irradiance profile within the PBR that conclusions could be drawn about the radiation history of the cells, and biokinetic expressions could be used to model growth over an appropriate period. Biokinetic simulations were carried out, and assumed that the growth behaved according to Monod kinetics. The expression for biomass concentration was updated with the time step used in the Lagrangian simulations. The computational power required for the two-flux model and biomass concentration was unfeasible, and simplifications were made. An astute observation found that for any number of cells, a similar radiation history and growth rate was observed. This led to an expression for averaging the growth rate. This meant that the system could be solved numerically in a matter of seconds. There are examples of other pieces of work which follow roughly the same methodology [58] **cite more examples**. In some previous studies [58], [90], a Lagrangian approach was used to simulate the growth of algae in a PBR using stochastic fluctuations based on [91]. This approach was similar to the previously discussed example. The radiative transfer equation however was simplified to the Beer-Lambert law, and the PSU model [85] was used. As discussed in Section 1.2.3, the Beer-Lambert approximation is not appropriate when the effects of in-scattering are important for the description of the system.

## 1.3 Research objectives and approach

Several research gaps have been determined in response to the suite of literature available since the beginning of this thesis. Photosynthesis process modelling techniques are generally well understood, especially when developed and validated against artificially irradiated photobioreactors. Biological process models fall into three main categories, labelled type I, II, and III [56]. These categories relate to their degree of complexity, especially when growth expressions are coupled to the radiative field. Type I models assume that all photosynthetic organisms are irradiated uniformly with an irradiance equal to that of the irradiated surface of a photobioreactor or the averaged irradiance within a solution domain. Type II models aim to decompose a solution domain into several subdomains of uniform irradiance. This means that the growth and productivity of a photosynthetic system can be described in terms of a light gradient. Type III models assess the light history of a photosynthetic particle, and describe the growth behaviour as the particles flow in and out of irradiated areas within a photobioreactor. This third type of model requires a description of the flow field as well as a light gradient to accurately determine biomass growth. Biological growth terms can consider either the photosynthetic microorganisms as a bulk single state, or as three different states depending on the perceived irradiance of the particles [85]. The latter biological model is the most widely used within process models for photosynthetic productivity. Despite the rich suite of process modelling and computational fluid dynamics approaches for algal biomass, there is no equivalent for purple phototrophic bacteria. With different metabolisms to those of algae, it is not sufficient to base PPB models off algal models. However, these can serve as inspiration when developing spatiotemporal models.

### **1.3.1 Research objective 1: A description of the process biokinetics of phototrophic systems**

The growth of PPB in a nutrient rich environment has not been described at the process level. With limitations such as non-trivial requirements for light energy, mixing energy, and harvesting challenges, a model with a higher level of abstraction than a metabolic pathway description is required.

A photo-anaerobic model (PAAnM) was developed to address these concerns. The model was based on the IWA semi-mechanistic family of models and used Monod expressions for nutrient and light limitations. The model was designed such that its extensibility to three spatial dimensions was possible.

### **1.3.2 Research objective 2: Computational fluid dynamics analysis of single and two-phase photobioreactors**

Based on the literature review, photosynthetic and phototrophic systems vary in space as well as time, due to irradiation and fluid flows. While algal CFD models have already been applied, few considered a coupled multiphysics solution, and the solution workflow of coupled solution procedures has been disjointed, with multiple simulation environments being used for models.

A modelling framework was therefore developed in OpenFOAM which included the coupling between single or multiphase flows, radiative transfer, and biokinetic behaviour of the phototrophic biomass.

### **1.3.3 Research objective 3: A multidimensional, phototrophic, continuum biofilm model**

Contributor	Statement of contribution	%
<b>Your Name</b>	writing of text	70
	proof-reading	60
	theoretical derivations	70
	numerical calculations	100
	preparation of figures	80
	initial concept	10
Co-author 1	writing of text	20
	proof-reading	10
	supervision, guidance	20
	theoretical derivations	10
	preparation of figures	20
	initial concept	10
Final Author	writing of text	10
	proof-reading	30
	supervision, guidance	80
	theoretical derivations	20
	preparation of figures	10
	initial concept	80

If your task breakdown requires further clarification, do so here. Do not exceed a single page.

# **Chapter 2**

---

## **A description of the process biokinetics of phototrophic systems**

---

Introduce the broad layout of the chapter.

### **2.1 Introduction**

Rewrite the contents of Daniel Puyol's paper to include my work here.

Contributor	Statement of contribution	%
<b>Edward M. Barry</b>	writing of text proof-reading theoretical derivations numerical calculations preparation of figures initial concept	60 10 60 100 80 40
Christopher T. DeGroot	writing of text proof-reading supervision, guidance theoretical derivations preparation of figures initial concept	20 20 40 30 0 0
Tim Hülsen	writing of text proof-reading supervision, guidance theoretical derivations preparation of figures initial concept	10 30 20 5 10 30
Damien J. Batstone	writing of text proof-reading supervision, guidance theoretical derivations preparation of figures initial concept	10 40 40 5 0 30

# **Chapter 3**

---

## **Computational fluid dynamics analysis of single and two-phase photobioreactors**

---

Modelling phototrophic systems is important for design, prediction and optimisation purposes. These systems differ from conventional process systems because the radiative field, necessary for phototrophic growth, is not uniform within the photobioreactor. As such, the common assumption of a well-mixed system cannot be applied. In this work, a computational fluid dynamics including biokinetics (bio-CFD) approach to photobioreactor modelling was developed for two reactor configurations (flat plate and cylindrical). The CFD models were compared to three other common modelling techniques: (a) completely mixed with a uniform radiative field set to the incident irradiance, (b) completely mixed with a reduced uniform radiative field determined at half the radius or equivalent, and (c) a mixed tank where the radiative field is dynamic and determined from particle irradiation incidence in a CFD analysis. The two mixed-tank approaches (model a and b) over-predicted growth rates compared to the full bio-CFD solution for both reactor configurations. The particle-radiation dynamics (model c) were in agreement with the full CFD solution for the cylindrical configuration, however deviated for the flat plate configuration. The reactor configuration influenced biomass growth rate for all models, despite the operating volume being equal. This highlights the importance of reactor geometry and incorporating spatial variations of the radiative field when modelling photobioreactors.

### **3.1 Introduction**

There has been an increase in interest in photobioreactor (PBR) systems in recent years as they have proven to be effective in waste treatment and resource recovery [?, 2] and renewable energy generation [5]. However, PBRs have not achieved major penetration in this sector, mainly due to high capital and operating costs, with effective light delivery being a major issue in both artificial and natural light systems. To offset these costs, research has shifted to the creation of valuable products instead of solely recovering nutrients. For example, complex organics, including pigments in algae [?] and purple phototrophic bacteria (PPB) have value, and they can be used to produce fertilisers and

animal feeds as microbial protein [92, 93]. Due to promise in multiple product lines, as well as the ability to treat wastewater purely through assimilation, PBRs will have an increased potential role in future resource recovery facilities.

One of the critical barriers to practical implementation of PBRs is that of size scaling [94], with light delivery at larger scale being a particular issue. This is due to the complex interactions between different physical processes occurring in PBRs. These include fluid hydrodynamics, radiation delivery, and biomass growth. A method to address this is by scaling prototype reactors. This approach is important, however effective modelling can accelerate development and lead to better reactor performance [95].

Several approaches to PBR modelling have been explored, with the majority of cases considering biokinetics as the controlling mechanism for process design and optimisation, generally implemented in a lumped parameter (*i.e.* completely stirred tank or plug flow) model [56, 96]. Distributed parameter modelling (*i.e.* the consideration of both spatial and temporal variations) have been considered in limited cases [23]. This means that the coupling between fluid flow, biokinetics and radiative transfer can be explored in more detail, and operational non-uniformities can be detected for given reactor designs without the need for physical prototyping [23]. Distributed parameter models have been successfully used to screen for problems in the scale-up of chemical process reactors [97]. Modelling is particularly useful when combined with computational fluid dynamics (CFD), generally implemented using a finite volume method (FVM) [22]. The FVM is generally favoured due to its ability to implement non-uniform grid discretisation and because states are inherently conserved. As such, the use of the FVM for PBR modelling has seen a substantial increase over recent years [23]. Publications related to this explore the coupling of the physics to varying degrees. Most of the available works are exercises in fluid flow description, only qualitatively (not explicitly) assessing the effect of the flow field on the biomass activity [?, 98, 99]. More rigorous studies exist, where the links between fluid flow, radiation, and biokinetics are explicitly simulated in the CFD framework. For example, previous work has looked at a multiphase hydrodynamic model integrating radiative transfer and algal biokinetics into both Eulerian and Lagrangian flow field specifications [?, 75]. The model could effectively represent experimental results, and demonstrated the useful nature of a multiphysics approach to PBR modelling. All studies considered to date have dealt with microalgal PBRs, and none have considered PPB (*i.e.* IR-driven systems) when developing PBR models.

Due to the spatially varying nature of the radiative field, it is likely that lumped parameter modelling approaches do not effectively describe the behaviour of PBRs. In cases where a complete-mixed assumption is made, and the modelling results are validated against pilot or large scale data. Growth and uptake parameters are aggregate and system-specific, rather than generalisable properties (*i.e.*, uptake or growth rate may depend on assumed intensity). Specifically, the exponentially decaying nature of the radiative field along a length dimension into the domain means that the acquired parameters are highly dependent on geometry, and may not be inherently related to biokinetics.

Despite potential improvements in PBR understanding due to CFD modelling, a disadvantage of this approach is the computational time and resources required. There is also limited description of

generalisable approaches and code in the literature. This paper attempts to address these limitations by developing a generalised reactive CFD approach to photobioreactor systems, and applying it in single and multiphase configurations. The CFD model describes the fluid hydrodynamics, radiative transfer and process biokinetics. As a lumped parameter model is commonly applied to PBR assessment, this is particularly assessed, to identify whether variations on lumped parameter modelling approaches can effectively represent the coupled multiphysics description provided by CFD simulations.

## 3.2 Methods

### 3.2.1 Geometry and mesh generation

Two test cases were assessed, both being infrared photobioreactors (PPB systems). The first case (Figure 3.1(i)) was a cylindrical 2 L stirred reactor (CR), which is a scaled-up representation of commonly applied mixed irradiated systems (*e.g.* static or agitated serum flasks [14]). The second case (Fig. 3.1(ii)), also a 2 L reactor, was a flat plate multiphase PBR (FPR) previously described [?, 2]. The CR was mechanically agitated with a vertical impeller, while the FPR was mixed through headspace gas (mainly nitrogen) with a sparging system in the base.

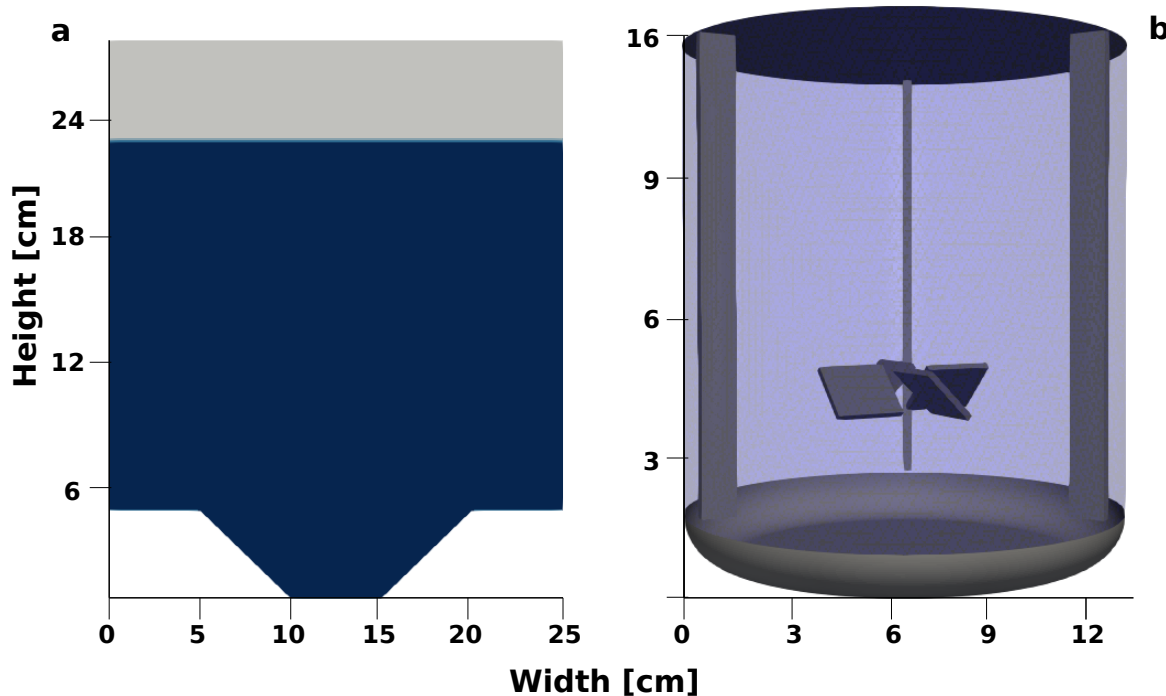


Figure 3.1: Representation of the geometries of the FPR (a) and the CR (b) upon which the simulations were based. The depth of the FPR is 6.0 cm. The blue region of the FPR represents the initial liquid volume fraction in the reactor, with the grey region representing the headspace. A single liquid phase was simulated in the case of the CR.

Both geometries were developed in the CAD package Salomé Méca [?]. The surfaces were meshed as 2-dimensional triangular meshes. A fine triangular surface mesh ( $\sim$  1 million discrete surfaces) was applied such that the geometries were watertight (*i.e.* there were no gaps in the tessellated surfaces) when used in the meshing process. The resulting meshes were exported as stereolithographic files as a basis for the volume meshes. Meshing was done using the cartesianMesh application, a hexahedral

dominant meshing utility belonging to the cfMesh library [?] which is built upon the OpenFOAM framework [?]. The meshes are presented in the supplementary material (S.1).

### 3.2.2 Fluid flow

#### Governing equations

It is assumed that the flow consists of an incompressible, Newtonian fluid under steady-state, isothermal conditions. The flow is considered to be turbulent and is modelled using the Reynolds-Averaged Navier-Stokes (RANS) equations with an appropriate turbulence model. The RANS equations are derived by decomposing the fluctuating velocity and pressure fields into their time-average plus an instantaneous fluctuation from the mean, i.e.

$$\mathbf{u}(\mathbf{x}, t) = \mathbf{U}(\mathbf{x}) + \mathbf{u}'(\mathbf{x}, t) \quad (3.1)$$

and

$$p(\mathbf{x}, t) = P(\mathbf{x}) + p'(\mathbf{x}, t) \quad (3.2)$$

where  $\mathbf{u}$  and  $p$  are the instantaneous velocity and pressure fields;  $\mathbf{U}$  and  $P$  are the time-averaged velocity and pressure fields; and  $\mathbf{u}'$  and  $p'$  are the instantaneous fluctuations in velocity and pressure from the mean.

For an incompressible fluid, the Reynolds-averaged conservation of mass equation is expressed as

$$\nabla \cdot \mathbf{U} = 0 \quad (3.3)$$

The RANS equations for the steady-state conservation of momentum is expressed as

$$\nabla \cdot (\mathbf{U}\mathbf{U}) = (\nu + \nu_T) \nabla^2 \mathbf{U} - \frac{1}{\rho} \nabla P \quad (3.4)$$

where  $\nu$  is the kinematic viscosity and  $\rho$  is the density of the fluid, which remain fixed for the cases considered in this study. The turbulent (eddy) viscosity,  $\nu_T$  results from the velocity fluctuations and represents the increased diffusivity due to turbulent mixing. Most often, two-equation turbulence models are used to determine the eddy viscosity, since they give a reasonable balance between accuracy and computational cost [22].

The eddy viscosity is defined through the Boussinesq hypothesis, given as

$$-\overline{u'_i u'_j} = \nu_T \left( \frac{\partial U_i}{\partial x_j} + \frac{\partial U_j}{\partial x_i} \right) - \delta_{ij} k \quad (3.5)$$

where the overbar represents a time-average,  $k$  is the turbulent kinetic energy, and  $\delta_{ij}$  is the Kronecker delta function. In practice, the eddy viscosity is defined by the solution of turbulence model

equations. Most often, two-equation turbulence models are used, which give a reasonable balance between accuracy and computational cost [22].

In this work, the  $k - \omega$  SST model of [47] is used. This model implements a blending between a  $k - \omega$  formulation in the near-wall region and a  $k - \varepsilon$  formulation in the free-stream region. This avoids the need for damping functions near the wall that are required for  $k - \varepsilon$  models and avoids problems with sensitivity to free-stream conditions that occur with standard  $k - \omega$  models.

The governing equation for the turbulent kinetic energy,  $k$ , is as follows [47]

$$\frac{\partial k}{\partial t} + \mathbf{U} \cdot \nabla k = \tilde{P}_k - \beta^* k \omega + \nabla \cdot [(\mathbf{v} + \sigma_k \mathbf{v}_T) \nabla k] \quad (3.6)$$

where  $\beta^*$  and  $\sigma_k$  are constants,  $\tilde{P}_k$  is the production rate of turbulent kinetic energy (with a production limiter applied to prevent build up in stagnation regions), and  $\omega$  is the specific dissipation rate. The dissipation rate is calculated in the  $k - \omega$  SST model using the following transport equation [47]

$$\begin{aligned} \frac{\partial \omega}{\partial t} + \mathbf{U} \cdot \nabla \omega &= \alpha S^2 - \beta \omega^2 + \nabla \cdot [(\mathbf{v} + \sigma_\omega \mathbf{v}_T) \nabla \omega] \\ &\quad + 2(1 - F_1) \sigma_{\omega 2} \frac{1}{\omega} \nabla k \cdot \nabla \omega \end{aligned} \quad (3.7)$$

where  $\alpha$ ,  $\beta$ ,  $\sigma_\omega$ , and  $\sigma_{\omega 2}$  are constants,  $S$  is the invariant of the strain rate tensor, and  $F_1$  is a blending function.

With the solutions of Eqs. 3.6 and 3.7, the eddy viscosity is then calculated according to

$$\nu_T = \frac{a_1 k}{\max(a_1 \omega, SF_2)} \quad (3.8)$$

where  $a_1$  is a constant and  $F_2$  is a blending function [47]. Values of all constants and auxiliary functions can be found in the work of Menter, 1994 [47].

The RANS equations also require wall functions to specify the near wall velocity when the viscous sublayer is not fully resolved by the mesh. The wall functions here implement a blending of viscous and log-law profiles, such that they are robust to mesh refinement, which is an important factor in separating discretisation and modelling errors [45].

### Hydrodynamic boundary and initial conditions

The initial conditions for the hydrodynamic model were zero gauge pressure and zero velocity at all points within the domains. At all walls, no-slip velocity boundary conditions were applied, along with zero gradient pressure conditions. When gradient conditions are applied at all walls, the pressure level must be set at some point within the domain. This is done internally in OpenFOAM by setting the gauge pressure to zero in a single (arbitrary) control volume. For the CR, a flow field was induced using four impeller blades pitched at 45°, spinning at 130 RPM. For the FPR, gas with the physical properties of nitrogen entered the domain at a rate of 6 L/minute through the inlet patches.

### 3.2.3 Radiative transport

#### Governing equations

Radiation delivery remains one of the major process bottlenecks to the design and effective operation of photobioreactors. There are many PBR CFD studies which treat the radiative field as a Beer-Lambert approximation, however this approach does not account for in-scattering phenomena. Failure to incorporate in-scattering in the CFD solution can lead to errors of as much as 20% [52]. The general form of the radiative transfer equation (RTE) accounts for the in-scattering effects, and is defined as

$$\frac{dI_\lambda(\mathbf{r}, \mathbf{s})}{ds} = \kappa_\lambda I_{b\lambda} - (\kappa_\lambda + \sigma_{\lambda,s}) I_\lambda(\mathbf{r}, \mathbf{s}) + \frac{\sigma_{\lambda,s}}{4\pi} \int_{4\pi} I_\lambda(\mathbf{r}, \mathbf{s}') \Phi_\lambda(\mathbf{s}, \mathbf{s}') d\Omega' \quad (3.9)$$

where  $I_\lambda$  is the spectral radiation intensity for wavelength  $\lambda$ ,  $\mathbf{r}$  is the position vector,  $d\Omega$  is a differential solid angle that is centred along the vector  $\mathbf{s}$ ,  $s$  is the distance along  $\mathbf{s}$ ,  $\kappa_\lambda$  is the spectral absorption coefficient, and  $\sigma_{\lambda,s}$  is the spectral scattering coefficient. The first term on the right accounts for black-body radiation. As we are accounting for either solar or artificial optical radiation, and relatively low temperatures of operation ranging between 4 °C and 40 °C, this term has been omitted from the solution. The second term on the right hand side accounts for absorption and scattering, which combine to create the extinction term. For each participating species within the liquid phase, we can include an extinction term, which sum to that shown in Eq. 3.9. The third term accounts for in-scattering through the phase function  $\Phi_\lambda$ .

There are several phase functions which have proven useful for photosynthetic media conditions: Henyey-Greenstein (HG) [68], truncated phase function (TPF) [52], and the Schlick model (SM) [84]. [84] found that in the field of computer graphics and animations, the Schlick model was less computationally expensive but was still able to approximate the effects of anisotropic scatterings to the same standard as the HG model. The Schlick model is defined as;

$$\Phi_s(k, \theta) = \frac{1 - k^2}{4\pi(1 + k \cos(\theta))^2} \quad (3.10)$$

where  $k \in [-1; 1]$  and  $\theta \in [0; \pi]$ . The parameter  $k$  implies an average cosine of scattered angles with a positive value giving preference to forward-scattering, a negative value giving rise to back-scattering, and a null value denoting isotropic scattering. The angle  $\theta$  is the scattering angle of a ray.

The implementation of the RTE in the form of Eq. 3.9 does not translate readily to photobioreactors, where multiple multiple participating species may exist, with different extinction coefficients. The expression has therefore been modified to include the participating species within a photosynthetic medium along with their specific absorption and scattering coefficients, which have been combined

into a global spectral extinction coefficient ( $E_j$ ) associated with each participating species  $X_j$ . The modified RTE, with the black-body radiation term omitted, is given as

$$\frac{dI_\lambda(\mathbf{r}, \mathbf{s})}{ds} = -\sum_j [E_{\lambda,j} X_j] I_\lambda(\mathbf{r}, \mathbf{s}) + \frac{\sigma_{\lambda,s,j}}{4\pi} \int_{4\pi} I_\lambda(\mathbf{r}, \mathbf{s}') \Phi_\lambda(\mathbf{s}, \mathbf{s}') d\Omega' \quad (3.11)$$

Custom software libraries, given the name `photoBio`, were written in order to extend or replace parts of the existing radiation libraries in OpenFOAM to suit the purpose of this study. As an example, in the standard OpenFOAM implementation, the radiative field is specified by temperature boundary conditions, while the irradiance can be specified directly in the customised solver. Another novelty in the custom `photoBio` library was that models needed to accept all participating media as input. The absorption and scattering expressions were therefore extended to allow for any number of species in a mixed-culture multiband system as shown in Eq. 3.11. Finally, the scope for the inclusion of phase scattering functions was adapted from previously built libraries of [68]. The Schlick model was added to this list of functionality, and was used for the cases shown in this study.

The particular method used for the resolution of the radiative field was the finite volume discrete ordinates method (fvDOM), renamed to `photoBioDOM` in the custom libraries that were written. The fvDOM is the conservative formulation of the discrete ordinates method [100], which allows the solution method to be implemented within the same finite volume framework as the flow and biokinetics models.

### Radiative transfer boundary conditions and parameters

An incident irradiance of  $30 W m^{-2}$  was applied to the outer walls of both the CR and FPR. A single wavelength band of peak  $850 \pm 5 nm$  was used for this simulation. Other important parameters governing the fvDOM angular discretisation and the biomass coupling were used in this simulation and are summarised in Table 3.1.

Table 3.1: FvDOM and biomass coupling parameters for the radiation component of the solution procedure

<b>Quantity</b>	<b>Value</b>	<b>Units</b>	<b>Meaning</b>	<b>Ref.</b>
$n_\phi$	6	-	azimuthal angle discretisation	-
$n_\theta$	6	-	polar angle discretisation	-
$n_{p,\phi}$	3	-	overhanging control azimuthal angle pixelation	-
$n_{p,\theta}$	3	-	overhanging control polar angle pixelation	-
$k$	0.98	-	Forward/back scattering Schlick asymmetry factor	[84], [?]
$a_{X_{PB}}$	106	$m^2 kg COD^{-1}$	absorption for a given <i>Rb. sphaeroides</i> (COD) biomass concentration at 850nm	[?]
$\sigma_{X_i}$	19	$m^2 kg VS^{-1}$	scattering for a given <i>Rb. sphaeroides</i> (COD), $X_S$ , and $X_I$ biomass	[?]

### 3.2.4 Biokinetic model

Biokinetics were taken from a lumped parameter model [96]. This considers growth of biomass and consumption of *COD*, *NH<sub>4</sub>N*, and *PO<sub>4</sub>P* but does not consider photon delivery. The state space includes three particulate state variables, PPB biomass, particulate composite biomass, and inert solids, as well as seven soluble state variables. All of these are represented as scalar differential variables. The governing equations for the solid and soluble state variables ( $\phi_i$ ) subject to advection, diffusion, and generation or consumption are as follows.

$$\frac{\partial \phi}{\partial t} + \nabla \cdot (\mathbf{U}\phi) - \nabla^2 \mathcal{D}_\phi \phi = r_\phi \quad (3.12)$$

where  $\mathbf{U}$  is the frozen velocity field of the fluid phase,  $\mathcal{D}_\phi$  is the diffusivity coefficient of scalar  $\phi$  in water, and  $r_\phi$  represents the generation or consumption terms, as previously defined in [96]. The diffusivity of the solid species was set to  $10^{-11}\text{m}^2\text{s}^{-1}$  for stability purposes.

The term  $r_\phi$  for each state variables includes a Monod term ( $\zeta_I$ ) with respect to irradiance (I) at any point in space (Eq. (3.13)). This means that the radiative field, and the biokinetic expressions have an interdependence which must be considered in the solution procedure.

$$\zeta_I = \frac{I}{K_I + I} \quad (3.13)$$

#### Biokinetic boundary conditions and parameters

Each scalar quantity in the biokinetic model was set to a uniform initial value. Zero-flux boundary conditions were specified for each wall in the domain for all state variables. Initial conditions are presented in the supplementary material (S.2).

### 3.2.5 Solution procedure

The solution procedure shows the order in which the governing equations are solved (Fig. 3.2). The momentum equations are solved until a quasi steady-state is found. This approach is applicable to both the single phase and multiphase systems. Secondly, for the multiphase system, the velocities for each phase are segregated. The single phase CR is not modified at this stage. Finally, the initial conditions for the biochemical equations are set, the radiative field is solved, and the biochemical equations are solved. The radiative field is updated every 15 minutes of simulation time.

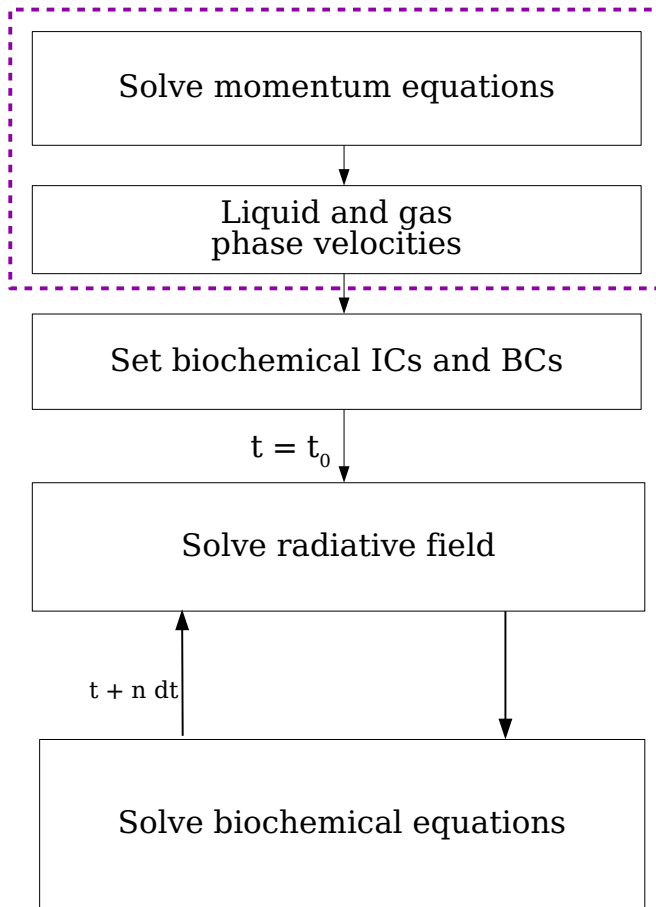


Figure 3.2: Solution algorithm for the solver. Momentum equations are solved until steady state is achieved and fed to the biochemical equation solver. The radiative field is updated every 15 minutes of simulated time.

The flow field is solved first. The assumption that the solid species do not participate in the flow field can be made for PBRs which have relatively low total suspended solids concentrations compared with other activated sludge processes [23]. The solver then enters a coupled radiation-biokinetics loop in which the radiative field is updated every 15 minutes of simulated time. A solution procedure that updated the radiative field at every time step was tested, but was prohibitively slow, and it was found to be unnecessary to update at such high frequency. Since the change in radiative properties due to biomass growth occur over an extended time frame, the update interval was found to not substantially influence the results.

The solver used for these simulations is the `pamFoam` solver: a multiphase, multiphysics implementation of a finite volume hydrodynamics, radiation, and biokinetics solver, which is built upon version 5.0 of the OpenFOAM framework, a collection of C++ libraries for solving continuum mechanics problems [?]. The solver and run-time dictionaries have been released under the AGPL-3 license, and can be accessed online (<https://gitlab.com/leboucher/pamFoam/tags/v5.1.0>). The

solver incorporates a custom radiation transport library built upon the finite volume discrete ordinates method [100], but adapted for use with phototrophic models. Its source code can also be found online (<https://gitlab.com/leboucher/photoBio/tags/v5.1.0>). The solid and soluble species were implemented as passive scalar transport equations.

### 3.3 Results and Discussion

#### 3.3.1 Radiative field dynamics

As the biomass grows in suspension over time, There is a decrease in intensity and distribution of the radiative field (Cf Eq. 3.11). This is shown in Fig. 3.3(a). This demonstrates that despite a similar radiation intensity, the geometry of the FPR is better than the CR, resulting in a higher average irradiation intensity, and a greater attenuation over time due to faster biomass growth. Fig. 3.3 also shows spatial distribution of radiative intensity at the start of the simulation, and at 24 hours. Sub-figures b and c correspond to the FPR, and sub-figures d and e show the CR. This demonstrates a substantial attenuation over time from  $12 \text{ Wm}^{-2}$  to  $7 \text{ Wm}^{-2}$  in the FPR and from  $5 \text{ Wm}^{-2}$  to  $3 \text{ Wm}^{-2}$  in the CR. The percentage decrease corresponded to an increase in the phototrophic biomass  $X_{PB}$  from  $0.5 \text{ g CODL}^{-1}$  to  $1.0 \text{ g CODL}^{-1}$  in the FPR and  $0.5 \text{ g CODL}^{-1}$  to  $0.8 \text{ g CODL}^{-1}$  in the CR over the same period of 24 hours. The change in other particulate species was relatively small over that same time period.

Findings from other studies [68] have shown that volumes within a reactor with an irradiance below  $2 \text{ Wm}^{-2}$  are effectively dark zones. Over time, self shading by biomass becomes apparent, which means that the fluid hydrodynamics become increasingly important if PBRs are to maintain substantial phototrophic biomass at high concentrations. For the FPR, the volume percentage of dark zones is 0%, compared with 30% for the CR. At 24 hours of simulated time, despite 25% more particulate matter, only 25% of the volume is in the dark, compared with 55% for the CR. Both the limitations in nutrient and photon availability mean that this proportion sees diminishing rates of biomass shading as the simulation continues. These results support other findings that in suspended biomass PBRs, the majority of the reactor is in the dark when operating at steady state with substantial phototrophic biomass and particulate concentrations. It is clear that for near infrared radiation, attenuation is more significant within the phototrophic media than in the gas phase, and both multiphase (gas-liquid) and single phase liquid systems were modelled, although a more thorough investigation around the bubble dynamics and their effect on the radiative field is required to quantify these interactions.

#### 3.3.2 Short-term particle radiation dynamics

The short term particle radiation dynamics result from the fluid field moving biomass particles within the heterogeneous radiative field as shown in Fig. 3.4. The first column (a,c) corresponds to the particle radiation dynamics of the FPR, with the same data being represented as a dynamic plot (a) and a frequency histogram (c). The second shows the parallel results for the CR. This demonstrates that

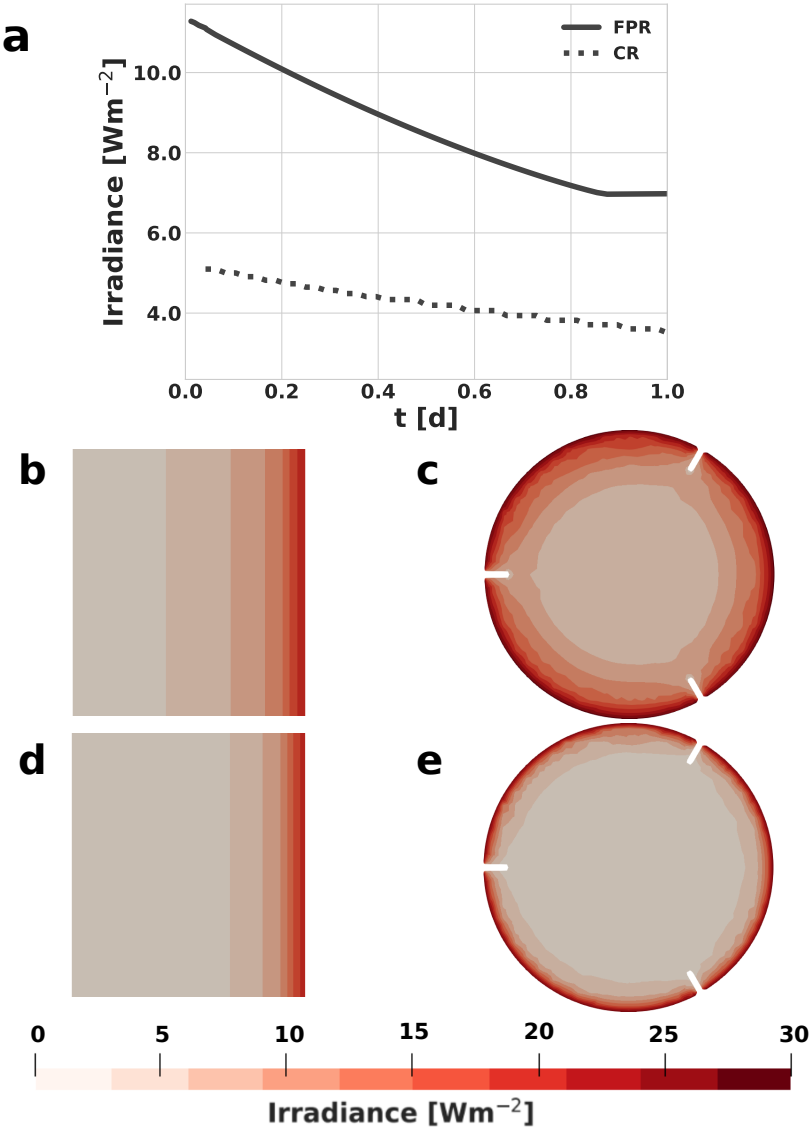


Figure 3.3: Evolution of the radiative field ( $\text{Wm}^{-2}$ ), volume averaged over all time steps, and the spatial changes over time for the FPR and CR. Cross-sectional view at reactor from 0 cm to 3 cm from the radiation source. (b,c) corresponds to the radiative field at the start of the simulation, and (d,e) is the radiative field at 24 hours for the FPR and CR respectively.

biomass in both reactors is subject to on-off irradiance cycles on the order of 3-5 s, with an amplitude of  $20 \text{ Wm}^{-2}$ . However, the dynamics are quite different, with particles in the FPR being irradiated for longer, and with a higher base-line ( $5 \text{ Wm}^{-2}$  in the FPR compared with  $0 \text{ Wm}^{-2}$  in the CR). This indicates that in the FPR, particles are effectively always irradiated at a minimum level, whereas in the CR, there is complete on-off cycling.

A question arising of the dynamic radiative field is whether the PPB biomass is sufficiently fast to respond to these changes. If the biomass response is much faster than the change in intensity, the growth kinetics can be treated as a continuous function (with dependence on intensity). If biomass response kinetics are also on the order of seconds, lower-level expressions would be required (which also consider photo-enzyme kinetics). The response time for *Rhodobacter sphaeroides* was determined in the literature to be in the order of  $10^{-11}$  seconds [?]; a time constant much smaller than the periods

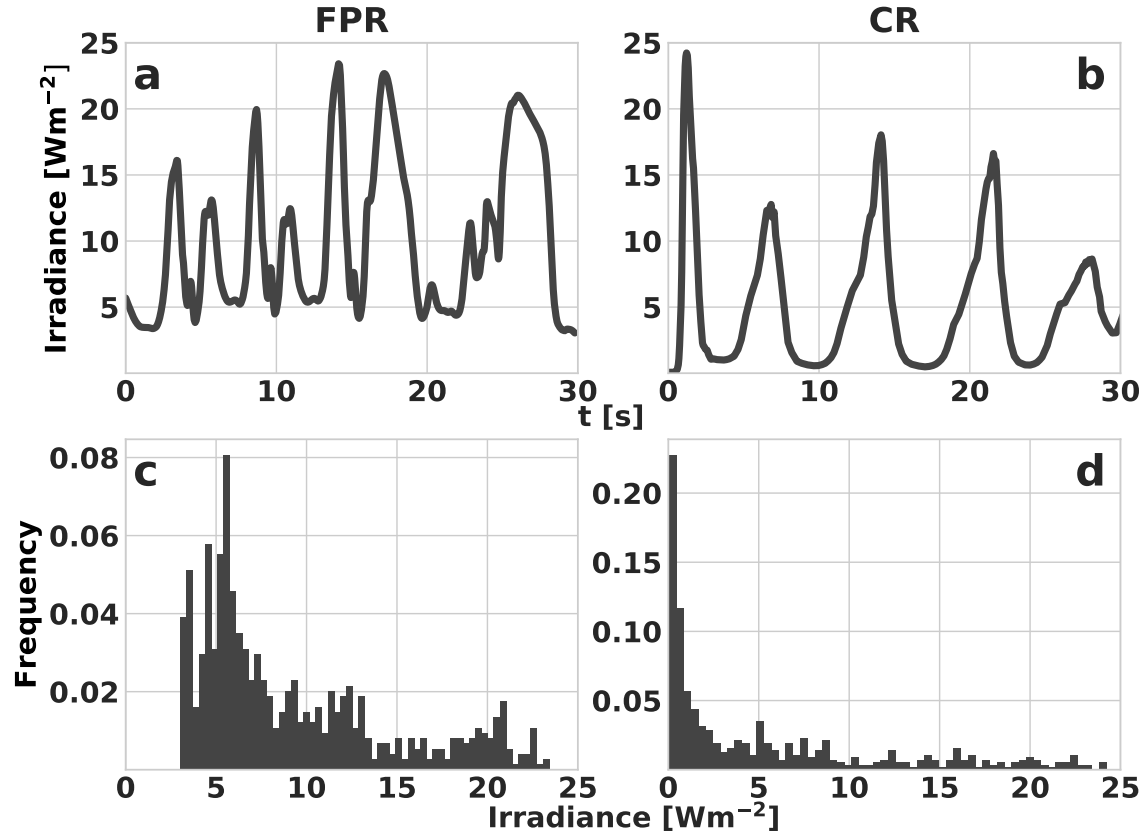


Figure 3.4: Particle radiation dynamics for an 850 nm band of irradiance. The top row (a, b) shows the transient radiative field experienced by a PPB particle for the FPR and CR reactors respectively. The same field is represented for both reactors (c, d) as a histogram on the bottom row. Both reactors have an incident irradiance of  $30 \text{ Wm}^{-2}$ .

seen in Fig. 3.4. Therefore, this justifies the use of a continuous function with respect to radiation for both this case, and in scaled-up systems, since they will generally have longer time constants due to the larger dimension with respect to velocity. This also justifies the approach used in this paper to generate results, with biomass growth coupled to the radiative field, and phototrophic organisms self-shading as they grow.

### 3.3.3 Growth of PPB biomass and uptake of soluble substrates

Four comparative simulations were done to assess the full Eulerian solution (as used so far in this paper - solution 4) to three reduced continuously stirred tank reactor (CSTR) versions. These include (for each reactor):

1. Uniform irradiance at incident value  $30.0 \text{ W m}^{-2}$  (ODE1). This is the standard approach that can be applied in a lumped-parameter model [56].

2. Irradiance fixed at the the volume-averaged value as presented at in Fig. 3.3(a). These values for the FPR and CR were  $11 \text{ W m}^{-2}$  and  $5 \text{ W m}^{-2}$  respectively (ODE2).
3. Dynamic irradiance as determined and presented in Fig. 3.4(a, b). This data is treated as a dynamic input to the lumped parameter model (ODE3). The main reduction in extent compared to a full CFD simulation is that the biomass/substrate do not need to be represented by scalars. In order to represent the effect of only modelling the liquid-irradiance system, the 30 s profile was replicated in time to 24 h rather than taking the full dynamic profile which includes long-term temporal light attenuation due to biomass growth.
4. Full Eulerian CFD solution (CFD).

In the first two cases, no CFD is required, while in the latter two cases, CFD is required to identify the particle radiation exposure pattern, and for the integrated model respectively. The first two cases were explored because certain studies have taken modelling approaches using lumped parameters based on single values of uniform irradiance, with little information as to the spatial distribution of the radiative intensity field. This has been applied using either the surface incident exposure [101, 102], or volume averaged irradiance [?, 103]. This can lead to an over-prediction when reporting growth rates.

The biomass concentrations (in mgCOD/L) are shown for the various modelling approaches for both systems (Fig. 3.5(a, b)). These demonstrate light-limited, fairly uniform growth rates towards the substrate depletion point where the growth stops (*i.e.* a batch system). The uniform irradiance approaches generally over-predicted growth rates, particularly in the cylindrical reactor (where irradiation was fundamentally less efficient). The dynamic exposure approach was generally effective in representing biomass profiles, but with a clear deviation with respect to the full CFD approach. Specifically, there were slightly slower growth rates for ODE3 vs CFD. This is somewhat surprising since the final attenuation is higher in the full CFD approach when compared with ODE3 (due to biomass growth), but could be explained by the fact that this attenuation is due to biomass exposure rather than water attenuation. Therefore the light is not "lost", but rather used during attenuation.

Fig. 3.5(c-f) shows the uptake concentration of soluble substrates of the same simulations. Again, the hybrid approach (ODE3) is most effective compared with CFD, but there are substantial deviations for all three ODE approaches. The large deviations for substrate  $S_{AC}$  (Fig. 3.5(c, e)) and  $S_S$  (Fig. 3.5(d, f)) are most likely caused by inhibition of each respective uptake process (photoheterotrophic uptake for acetic acid, and for other organics) caused by the presence of the other soluble compound class. This, combined with the difference in uptake rates for acetate uptake ( $2.4 \text{ d}^{-1}$ ) and photoheterotrophic uptake ( $1.4 \text{ d}^{-1}$ ) [96] mean that based on the amount of light available in the system, different behaviour can occur.

The full ODE approach (ODE1, ODE2), as stated above, is the most common approach, taking either surface irradiation [101, 102], or an approximated reduced average irradiance [?, 103, 104]. This provided unsatisfactory results, particularly in the simplified CR. With respect to growth rates, and in

an actual system, these variations would be absorbed by biochemical parameters, making them non-transferable to other systems. A system can only be effectively approximated with a lumped parameter modelling approach if the reactor is not only well mixed, but also well serviced with a uniform irradiance which can be measured effectively. This would likely not be an effective photobioreactor field design, but these factors also mean that some care must be taken even in laboratory systems when determining biological parameters, since the surface measured irradiance will almost certainly not be the *in situ* irradiance. This would have an impact on biomass growth parameters.

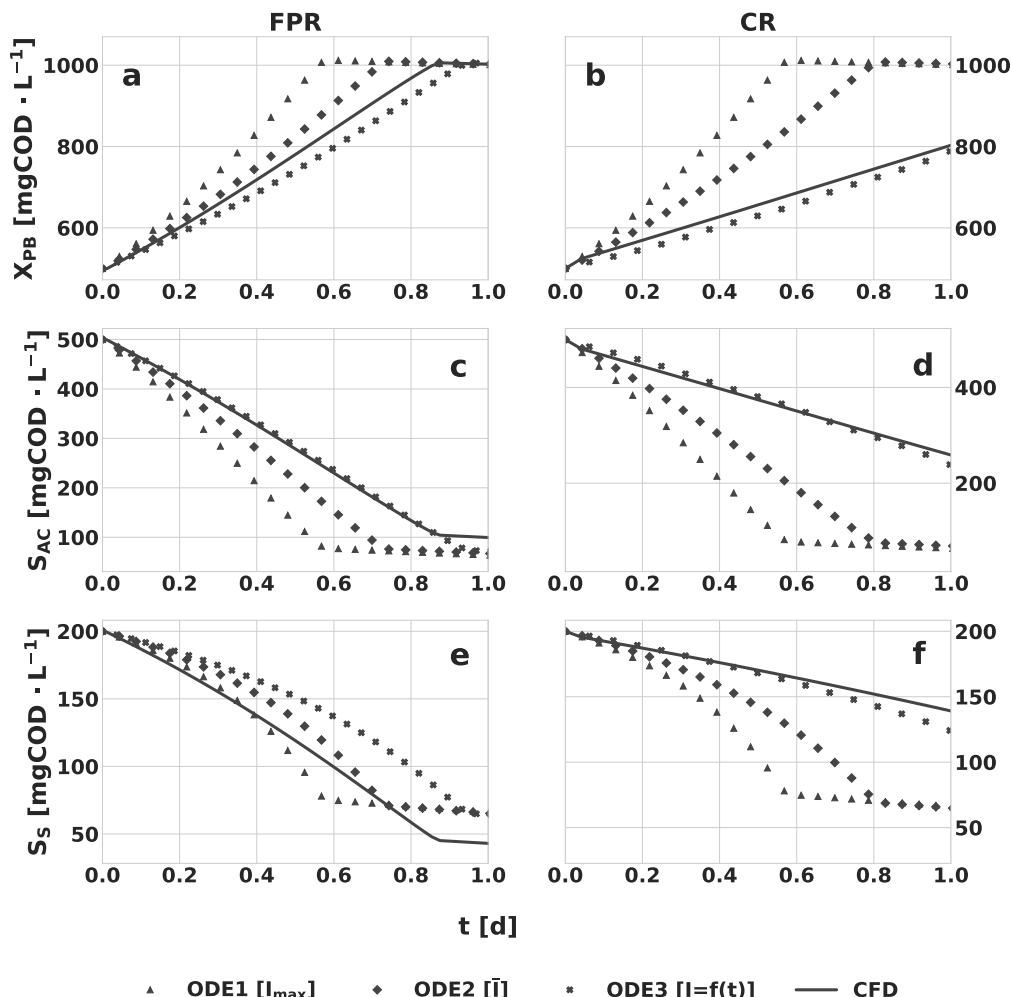


Figure 3.5: Biomass growth and substrate uptake for the FPR (a, c, e) and the CR (b, d, f). The first row shows the growth of PPB and the second and third rows show the consumption of acetic acid and other readily biodegradable soluble organics respectively. For all figures, the triangles correspond to ODE1, the diamonds correspond to ODE2, the crosses represent ODE3, and the solid line is the CFD solution.

The dynamic irradiance approach (ODE3) was far more effective in biological simulation, but the irradiance profile changes in each case, and cannot effectively represent irradiance changes as biomass experiences long-term growth. This has quite complex impacts, including potentially a loss in efficiency due to reduced biomass based attenuation. When compared with the full Eulerian solution

(CFD), the dynamic irradiance solution has a slightly slower growth rate, but the time constant is similar for both simulations. The hybrid approach therefore has some value, particularly where a full model cannot be formulated. However, the full model provides complete interpretation at a modest increase in computational complexity.

### 3.3.4 Limitations of the model

#### CFD considerations

There are three main limitations of the study with respect to the CFD implementation. Firstly, while gas and liquid phases have been modelled and biochemical state variables have been segregated in the liquid phase, the effect of biological activity on the gas field have not been incorporated. The mass transfer between phases was also not considered in this case. Including mass transfer models is important for photoautotrophic (gas fed) or photosynthetic ( $\text{CO}_2$ ) growth. Any mass transfer model is dependent on how the dispersed gas field is solved. Here, a uniform bubble Eulerian approach was taken, but an alternative that considers bubble size distribution such as population balance modelling could lead to an improvement in prediction of mass transfer. A better represented bubble size distribution would also allow analysis of its dynamic effects on the radiative field. This model considers planktonic biomass modelled as passive scalars. The momentum coupling would not substantially change interaction with the radiative field. However, an important possible extension is the inclusion of a spatially explicit biofilm. The current model lends itself well to include a continuum based biofilm model as a module in a broader continuum-based phototrophic growth model.

As the biomass has been implemented as passive scalars, the effects of changes in biomass concentration on the flow fields have not been quantified (*i.e.*, does not affect rheology, density or momentum). This could be incorporated through an upgrade of the biomass from scalar to dispersed phase. Modelling the solid system in a Lagrangian framework can also link the particulate species with a set of physical information, such as particle density and diameter. The particulate species as they are currently modelled could also be linked to a particulate density, which would then have an effect on the flow field.

#### Biochemical system limitations

This system differs from photosynthetic algae or cyanobacteria, where photosynthetic organisms may be in multiple states (excited, photoinhibited or resting) [56]. The state depends on the radiative intensity and the light history of the organisms. In addition, nitrogen storage becomes an important factor [105]. The short-term particle radiation dynamics as observed here are even more important in photosynthetic systems, where the transition in biological state adds another system dynamic which is on the same speed order as the cycling speed. Therefore, consideration of photo-dynamics is even more important when simulating white light systems, since, as discussed above, enzyme response is extremely fast (and photo-dynamics do not interact with this), while a change in photo-state is far slower. Photo-inhibition is another important factor not considered in the current model. The current

system was irradiated with  $30 \text{ Wm}^{-2}$ , and photo-inhibition has been reported to start occurring closer to  $900 \text{ Wm}^{-2}$  [106]. Updating the model to include photo-inhibition terms would increase the range of applicability of the model to outdoor PBR systems, and is an important factor for white light systems as discussed above. The time constant for recovery from photo-inhibition may make this a more complex response function, and increase the importance of considering photo-dynamics.

This model was simulated looking at a single radiation band at 850 nm. In reality, the growth of PPB depends on other wavelength bands, including 375 nm and 590 nm (facultative carotenoids) and the near infrared band ranges from 830 nm to 900 nm [?]. Upgrading the biochemical model to include the growth on several different wavelengths would lead to resolution of important aspects, including increased and differential attenuation of higher energy radiation. However, assigning fixed behaviour to organisms which can adapt to different environmental conditions, such as the growth or loss of chromophores due to low or high intensity radiative fields, means that there will always be a level of uncertainty which cannot be described by the model.

## 3.4 Conclusions

This study has looked at two different reactor setups; a flat plate reactor (FPR) and a cylindrical reactor (CR). Over these two different reactor geometries, four modelling approaches were evaluated;

1. ODE1: An ODE system taking a uniform radiative field equal to that of the incident irradiance.
2. ODE2: An ODE system taking a uniform radiative field equal to its value halfway into the domain as solved by the radiative transfer equation here, or alternatively by a Beer-Lambert relationship.
3. ODE3: An ODE system taking as input a dynamic irradiance experienced by a particle as it is carried by the velocity
4. CFD: A full Eulerian CFD approach accounting for fluid flows, radiative transfer, and the system of biochemical

The first two approaches tended to over-predict growth rates, meaning that the spatial variations within PBRs are important to consider, and local effects can have an impact on the overall solution. The results for ODE3 were similar to those for the full Eulerian CFD solution, irrespective of reactor geometry. This approach presents an appropriate compromise when computational resources are scarce, however the full Eulerian approach provides the complete interpretation for the PBR systems, with scope to expand on this model with more physical processes.

Several limitations to the study were identified, and were classed in two categories; CFD limitations and biochemical modelling limitations. The CFD limitations were that mass transfer in multiphase systems was not solved, and the model was developed as a planktonic model with passive scalars, limiting the description of physical processes such as biofilm development and effects on the flow field due to changes in density. The biochemical limitations extended on previous work to highlight

the adaptive changes of pigment production in response to the radiative field, and the effects of photoinhibition on uptake rates.

Contributor	Statement of contribution	%
<b>Edward M. Barry</b>	writing of text proof-reading theoretical derivations numerical calculations preparation of figures initial concept	70 60 70 100 100 60
Christopher T. DeGroot	writing of text proof-reading supervision, guidance theoretical derivations preparation of figures initial concept	20 10 20 10 20 10
Shakil Ahmmmed	writing of text proof-reading supervision, guidance theoretical derivations preparation of figures initial concept	20 10 20 10 20 10
Tim Hülsen	writing of text proof-reading supervision, guidance theoretical derivations preparation of figures initial concept	10 30 80 20 10 80
Damien J. Batstone	writing of text proof-reading supervision, guidance theoretical derivations preparation of figures initial concept	10 30 80 20 10 80

# Chapter 4

---

## A multidimensional, phototrophic, continuum biofilm model

---

Abstract

### 4.1 Introduction

#### 4.1.1 Processes governing the biofilm lifecycle

Biofilms are communities of bacteria, algae, protozoa, fungi and other microorganisms attached to a surface, and growing in an array of extracellular polymeric substances [?]. The lifecycle of a biofilm can be defined by the following processes:

1. Initial attachment to the substratum surface
2. Maturation of the biofilm
3. Detachment of biomass

The processes governing attachment are complex and varied. The physical properties of the solid substratum such as roughness, effective surface area, and hydrophobicity, play a role in the effectiveness of the attachment of microorganisms [?]. The ability of the surface to accept conditioning films (or protein rich coatings) and characteristics of the surrounding medium are also important factors for biofilm attachment [?]. Hydrodynamic behaviour is also important for the attachment of cells. Until a certain critical shear stress where detachment occurs, cells have a higher probability of adhering to a surface the more times they come into contact with that substratum. This means that turbulent flow regimes are more conducive to biofilm attachment [?].

Planktonic organisms secrete chemical signals, however due to the dispersed distribution of suspended biomass, these signals have very little effect on genetic expression. Conversely, due to the dense distribution of organisms in the attached biofilm layer, maturation of the biofilm is influenced by

quorum sensing, where the genetic expression of biofilm dwelling organisms is modified by chemical secretions of neighbouring organisms [?]. The change in genetic expression leads to different behaviours in the biofilm. During biofilm formation, extracellular polymeric substances (EPS) are formed which lead to some benefits for the biofilm; *a*) it acts as an adhesive for arriving organisms to the biofilm, *b*) it forms protection from antimicrobial substances, leading to a resilience in the biofilm, and *c*) it allows for transport of nutrients into the biofilm. As the biofilm continues to grow and expand, micro-niches form due to spatial variations such as nutrient diffusion and gas transfer limitations (anaerobes tend to aggregate near the biofilm-boundary layer interface, whereas anaerobes aggregate in oxygen poor environments. For photobiofilms, the consideration of the radiative distribution is also of interest as its attenuation could also affect the spatial distribution of photoorganisms within a biofilm [107].

The detachment of biomass occurs largely due to mechanical stresses. Erosion and sloughing occur depending on the nature of the flow field and boundary layer, and the shape and distribution of the biofilm itself. As detachment rates increase and balance growth rates, the biofilm remains in a quasi steady state [?, ?].

### 4.1.2 Examples of beneficial and harmful biofilms

It is important to understand the mechanisms of biofilm formation, whether the biofilm be beneficial or harmful. Examples of beneficial biofilms in process engineering applications include for the bioremediation of contaminated soils [?] and wastewater treatment applications where nutrients and impurities are removed from water streams through trickling filters or other engineered designs. Another application of interest in biotechnology is where biofilms aid in the harvesting of protein-rich bacteria, effectively short-cutting the need for expensive separation equipment associated with biomass thickening and dewatering [?].

On the other hand, bad biofilms can also have such effects as reducing process equipment efficiency, being dangerous, harmful, or completely pernicious [?]. Examples include the fouling on heat transfer and membrane equipment leading to a reduction in process performance [?], the formation of biofilms in food cultivation and preparation areas [?]. The control of biofilms is vitally important in the health industry, as they present themselves as sources for inflammation, impaired healing, antimicrobial resistance, and patient death [?]. As biofilm formation and growth can have significant positive or negative effects on society, the modelling of these systems is important in order to understand the details of the governing processes, therefore prevail in controlling such formation in practical applications.

### 4.1.3 Modelling of photobiofilms

Biofilm models which capture the heterogeneities and spatio-temporal variations are *de rigueur*. They are known as third generation models according to the IWA's task group on biofilm modelling. They

build on the previous classes of biofilm modelling where steady-state, homogenous biofilms were defined in order to describe mass transport between biofilm and bulk flow (first generation) [?]. Second generation models included updates to account for non-uniformities in the biofilm by describing microbial interactions. Third generation models can be described as either based on discrete agents, or as continuum models [?]. Each approach has its own benefits and drawbacks.

### **Discrete biofilm models**

There are two major discrete modelling approaches for biofilm formation: cellular automaton and agent based models. Cellular automaton models consist of discretising the spatial domain into discrete squares or cuboids for 2D or 3D models respectively. Each discrete element can be either occupied by a microbial cell, or a substance of interest, or can be empty. The cells are subjected to simple, discrete biological or physical operations [?]. The operations, or rules, can include substrate diffusion, biokinetics expressions such as growth and decay, and attachment and detachment processes [?]. Broadly accepted advantages of cellular automaton (CA) approaches are that the model setup oftentimes offers a simpler development cycle as it is based on a series of discrete steps. In addition, the implementation of irregular boundary conditions is easier with this method [?], and the approach is known to be relatively simple to implement across multiple computing processors when compared to differential descriptions of states [?]. There are several disadvantages to the CA method, including the fact that conservation is not maintained under substrate uptake and growth processes, and the biofilm advances based on the availability of unoccupied cells. This means that dynamic growth and transformation processes closer to the substratum are often ignored [?]. Additionally, as cells are effectively placeholders for physical information, the mesh cells are often of uniform physical state. The accuracy is therefore dependent on the resolution of the meshed domain [?].

The other main method of discrete biofilm modelling is the agent based modelling (ABM) approach. This technique is similar to the CA approach insofar as it incorporates a set of rules that biomass follows. However, it differs in that the representation of biofilm species is as particulate matter, which can occupy any point in continuous spaces. Constraints due to the discretised CA lattice do not apply. Agent based models have been used to describe the interactions between multispecies particulates, including EPS formation and its effects on the biofilm structure [?]. As the physical complexity of the modelled biofilm system increases, brute-force ABM simulations of complex systems often encounter computational limitations, limiting the spatial scale of ABMs. To overcome this limitation larger particles representing fractions of inert and active biomass has been presented. This type of model still follows ABM methods, with free-flowing particles, but the particles act as aggregate placeholders for physical information, similar to the CA methods [?].

Discrete approaches allow for the construction of complex models by building series of simple constraining rules. Model results often lead to a general idea of how the biofilm structure is formed, however agreement with experimental data is frequently case-specific [?]. This is due to the description of the physical phenomena being based on a set of simple instructions with aspects of stochasticity.

The order in which these instructions are executed can influence the results of the model, as well as the random nature of the discrete operations mean that results from identical initial conditions can differ significantly. Consequently, rigorous statistical analysis must be conducted in order to confirm the results from discrete models [?].

### Continuum-based biofilm models

Continuum-based biofilm models can be classed into two main categories; one dimensional models (1D) and multidimensional models (2D for domains in  $\mathbb{R}^2$ -space and 3D for domains in  $\mathbb{R}^3$ -space respectively). Perhaps the most widely used 1D biofilm model is the AQUASIM implementation [?] which builds upon the groundwork of [?] [?]. This model considers a multispecies competition and distribution within a biofilm. Included in the model are attachment and detachment processes, as well as considerations of mass transfer of soluble substrates within the porous structures. 1D biofilm model best lend themselves to particular cases: *i*) in educational or demonstration settings, *ii*) as part of broader or plant-wide models where mass exchange between biofilms and soluble substrates is to be quantified, but where computational requirements are to be used sparingly [?].

Multidimensional biofilm models are able to capture non-uniformities in the plan parallel to the surface substratum. Through this approach, one can explore the interactions between several species within a biofilm. Also, 2D and 3D approaches allow for analysis of time and space-dependent physical parameters and variables such as species and other particulate distribution, pressure gradients, and the interactions between soluble species and the porosity of the biofilm structure [108]. Demonstrations in 1D and 3D test cases with varying symmetric and asymmetric boundary conditions were run, and the assessment of biofilm growth was found to agree well with experimental results. [109], ([109]) also recognised the limitations associated with discrete models or 1D continuum models and thus proposed an extension to the Wanner-Gujer model as implemented in AQUASIM [?]. The model linked a biomass volume fraction to Monod growth kinetics. The changes in volume fraction described changes in pressure which was the driver of biomass spreading. As the biofilm front represented a boundary and was dynamic, interface capturing was achieved with the level-set method, which allows for the reconstruction of the biomass front from a differential distance function. 2D and 3D simulations were carried out, and the results showed the formation of microbial niches due to substrate gradients. This model represents one of the first examples of a mathematically rigorous approach being taken to biofilm modelling.

### Photobiofilm models

As the field of study of photobioreactors is in its infancy, the benefits of photobiofilm reactors have seldom been discussed. It has been identified that the harvesting, thickening and dewatering costs associated with phototrophic processes could be reduced if growth by attachment was the dominant growth mode in photobioreactors [?]. Purple phototrophic bacteria (PPB) are known to form heterogeneous, somewhat stratified biofilm structures in benthic zones of aquatic environments [?],

however algal biomass has proven more difficult to engineer into biofilm formations. A recent attempt to foster a mycoalgal biofilm proved to be more effective than in the axenic cultures [110], but for applications such as waste treatment, one doesn't have the privilege of being able to select specific co-cultures. That said, whatever the application of photobiofilm systems, that elucidation of the process kinetics coupled with biofilm development is required for a deeper understanding, especially with respect the coupling with the radiative field.

With regards to phototrophic biofilm modelling, only two examples exist prior to this work. The first phototrophic biofilm (PBF) model was proposed as a two dimensional application to a porous substrate photobioreactor (PSBR) [111]. The model looked at the productivity of *Anabaena variabilis*, a cyanobacterium, through substrate transport, photon delivery, and growth processes. There was good agreement between numerical simulations and experimental results with respect to biomass productivity over a range of thicknesses between 35  $\mu\text{m}$  and 45  $\mu\text{m}$ . This model focused on a pure culture of cyanobacteria, and the evolution of biofilm structure was not explored in this scope. Additionally, variations in soluble substrate concentrations into the biofilm towards the surface substratum were not presented.

The second study focused on a 1D application of a PSBR [77]. This model extended the previously mentioned study with respect to the substrate gradients perpendicular to the biofilm surface substratum. The radiative transfer equation was used to simulate the light delivery to the biofilm concluded that phase in-scattering and pigment adaptation were important considerations. The advection of the biofilm front was by treating the biomass length as a discrete quantity, either consuming or releasing discrete elements at each simulated time step.

The proposed model in this paper differs from the previous PBF examples in the following aspects:

1. Biofilm models should be developed for implementation in all spatial dimensions. Decisions to simplify the model should be made by the user at implementation. Presented here is a multidimensional phototrophic biofilm model.
2. The evolving structure of the biofilm must be captured. The advancement of the biofilm front is coupled to biomass growth and decay processes. The interface between biofilm and liquid is captured by a conservative, coupled volume-of-fluid (VoF) and level-set method.
3. Biofilms are heterogeneous in nature. Scope must be made to model multispecies biofilm evolution. As such, presented here is a multidimensional, multispecies, dynamically structured phototrophic biofilm model.

In addition to these three points of novelty, the biofilm model has been implemented in OpenFOAM, a computational fluid dynamics (CFD) finite volume method (FVM) framework. This package is a collection of C++ libraries which allow for the resolution of continuum mechanics problems. The model extends on previous work by the authors [96]. The global purpose of this study is to explain the

physical phenomena occurring within biofilms so that subsequent studies can progress the work for design or prediction purposes.

## 4.2 Problem description

The modelling approach is concerned with the description of a phototrophic biofilm system consisting of purple phototrophic bacteria (PPB). The model description for this system has been previously described [96], however this did not account for spatial variations, and by extension, biofilm formation was not considered. The phototrophic biofilm grows attached to a surface substratum. Above the biofilm is a body of nutrient-rich liquid. Incident photons of wavelength 850 nm are irradiated from either  $\Gamma_0$  or  $\Gamma_3$  into the domain  $\Omega$ , as shown in Fig. 4.1. The initial thickness of the biofilm is 50  $\mu\text{m}$  with uniformly distributed solid species. The factor of incident irradiance is also explored, with three different irradiance levels of  $10 \text{ W m}^{-2}$ ,  $30 \text{ W m}^{-2}$ , and  $100 \text{ W m}^{-2}$  being simulated from the surface substratum. Incident irradiance in all cases is assumed uniform and diffuse across the whole boundary.

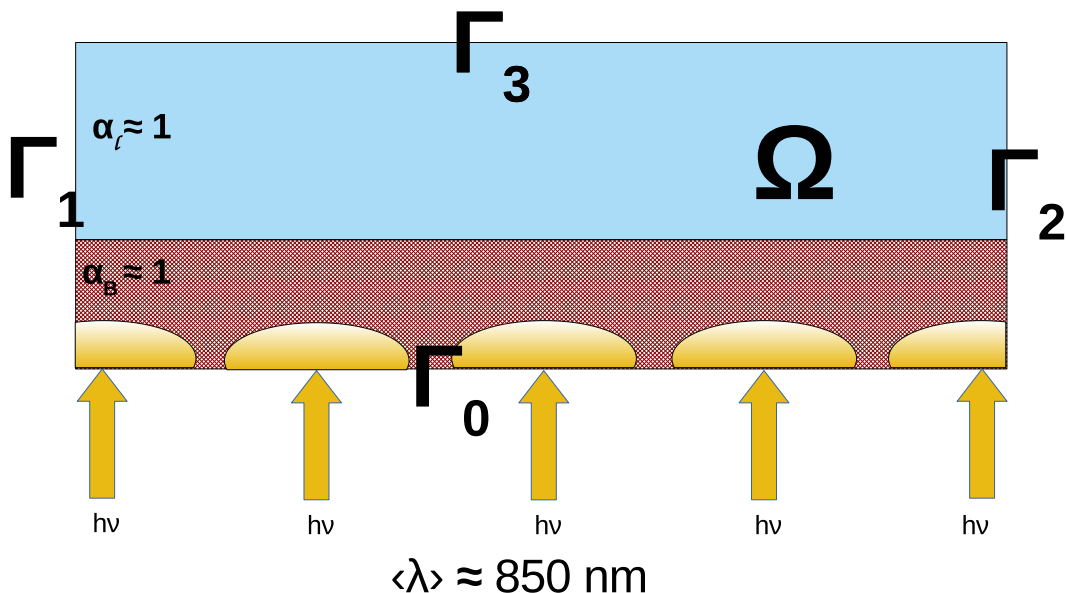


Figure 4.1: Two-dimensional representation of the simulation domain for the case of a bottom-irradiated biofilm. Boundaries  $\Gamma_4$  and  $\Gamma_5$  are out of, and into the page respectively, and take the same boundary conditions as boundaries  $\Gamma_1$  and  $\Gamma_2$ . The irradiance source ( $h\nu$ ) is in fact uniform and diffuse across the whole boundary. Subscripts relating to  $\alpha$ , namely **I** and **B** correspond to liquid phase fraction, and biofilm phase fraction respectively.

## 4.3 Mathematical formulation

### 4.3.1 Radiative transfer

The general form of the radiative transfer equation (RTE) has been adapted to phototrophic systems **cite me** [68], and includes the dependency on the concentration of solid species and water. The black body radiation term has been omitted from this equation due to minimal influence on the system energy balance (Eq. 3.11).

$$\frac{dI_\lambda(\mathbf{r}, \mathbf{s})}{ds} = -\sum_j [E_{\lambda,j} X_j] I_\lambda(\mathbf{r}, \mathbf{s}) + \frac{\sigma_{\lambda,s,j}}{4\pi} \int_{4\pi} I_\lambda(\mathbf{r}, \mathbf{s}') \Phi_\lambda(\mathbf{s}, \mathbf{s}') d\Omega' \quad (4.1)$$

where  $I_\lambda$  is the spectral irradiance for a given wavelength,  $\mathbf{r}$  is the position vector of a radiative ray,  $\mathbf{s}$  is the direction vector of the ray, and  $s$  is the path length. The first term on the right hand side is the extinction term, with  $E_{\lambda,j}$  being the specific extinction coefficient (the combination of scattering and absorption components) for participating species  $X_j$ . The second term on the right hand side is associated with in-scattering, where  $\sigma_{\lambda,s,j}$  is the scattering coefficient, and  $\Phi_\lambda$  is the wavelength scattering function from path  $\mathbf{s}$  to scattered direction  $\mathbf{s}'$  through solid angle  $d\Omega$ . The phase scattering function,  $\Phi_\lambda$  for this model is the Schlick function (Eq. 3.10), which is appropriate for optically thick media [84].

$$\Phi_s(k, \theta) = \frac{1 - k^2}{4\pi(1 + k \cos(\theta))^2} \quad (4.2)$$

where parameter  $k$  takes values between -1.0 and 1.0 included, with negative or positive values corresponding to back-scattering and forward scattering respectively. A value of 0 means scattering is isotropic. The parameter  $k$  represents the average cosine of the scattered angles. The angle  $\theta$  is that made by the previous path and scattered path of a ray.

### 4.3.2 Consumption and release of soluble substrates

Soluble substrates exist in both the volume of liquid, and the biofilm volume. Their growth and release expressions (hydrolysis of biodegradable particulate organic matter) have been previously described [96]. The soluble substrates considered in this study are readily biodegradable soluble organics expressed in chemical oxygen demand (COD), acetic acid (COD), hydrogen (COD), inorganic carbon (C), inorganic nitrogen (N), inorganic phosphorus (P) and soluble inert material (COD). The general form for the soluble balance equation is expressed in Eq. 4.3.

$$\frac{\partial S_i}{\partial t} = \mathcal{D}_i \nabla^2 S_i + r_i \quad (4.3)$$

where  $S_i$  is the soluble species  $i$ ,  $\mathcal{D}_i$  is the diffusion coefficient of species  $i$ , and  $r_i$  is the corresponding consumption/release equation [96].

### 4.3.3 Growth of particulate matter

The growth of particulate matter forms the biofilm structure and influences the pressure equation which influences advection of the biofilm front. The particulate species included in this study are PPB, slowly biodegradable particulate organics, and inert particulate organic matter. Similarly to [109], replace  $X_i$ , the concentration of particulate species  $i$  with  $\rho^* \theta_i$  where  $\rho^*$  is the density of particulate species, assumed constant for each species, and  $\theta_i$  is the volume fraction of species  $i$ . The growth terms for the particulate balance equations (Eq. 4.4) have been previously defined [96].

$$\frac{\partial \theta_i}{\partial t} = \lambda \nabla p \cdot \nabla \theta_i + \frac{g_i}{\rho^*} - \theta_i \sum_{i=1}^{N_{\theta_i}} \frac{g_i}{\rho^*} \quad (4.4)$$

where

### 4.3.4 Pressure term

The pressure term drives the advection of the biofilm front. It depends on the growth or decay of the solid species. All terms in this equation (Eq. 4.5) have already been defined.

$$-\nabla^2 p = \sum_{i=1}^{N_{\theta_i}} \frac{g_i}{\rho^*} \quad (4.5)$$

### 4.3.5 Boundary and initial conditions

These need to be included once debugging has finished.

## 4.4 Numerical Treatment

## 4.5 Implementation

## 4.6 Discussion

## 4.7 Conclusions



## **Chapter 5**

---

### **Conclusions and outlook**

---



---

# Bibliography

---

- [1] I. G. Minkevich, T. V. Laurinavichene, and a. a. Tsygankov. Theoretical and experimental quantum efficiencies of the growth of anoxygenic phototrophic bacteria. *Process Biochemistry*, 39(8):939–949, 2004.
- [2] T. Hülsen, E. M. Barry, Y. Lu, D. Puyol, J. Keller, and D. J. Batstone. Domestic wastewater treatment with purple phototrophic bacteria using a novel continuous photo anaerobic membrane bioreactor. *Water Research*, 100:486–495, 2016. Publisher: Elsevier Ltd ISBN: 0043-1354.
- [3] T. Hülsen, K. Hsieh, Y. Lu, S. Tait, and D. J. Batstone. Simultaneous treatment and single cell protein production from agri-industrial wastewaters using purple phototrophic bacteria or microalgae – A comparison. *Bioresource Technology*, 254:214–223, Apr. 2018.
- [4] C.-X. Sun, W.-N. Xu, X.-F. Li, D.-D. Zhang, Y. Qian, G.-Z. Jiang, and W.-B. Liu. Effects of fish meal replacement with animal protein blend on growth performance, nutrient digestibility and body composition of juvenile Chinese soft-shelled turtle Pelodiscus sinensis. *Aquaculture Nutrition*, 22(2):315–325, 2016.
- [5] A. Adessi and R. De Philippis. Photobioreactor design and illumination systems for H<sub>2</sub> production with anoxygenic photosynthetic bacteria: A review. *International Journal of Hydrogen Energy*, 39(7):3127–3141, 2014. Publisher: Elsevier Ltd.
- [6] W.-S. Liu, Y.-D. Kuan, K.-H. Chiu, W.-K. Wang, F.-H. Chang, C.-H. Liu, and C.-H. Lee. The Extract of Rhodobacter sphaeroides Inhibits Melanogenesis through the MEK/ERK Signaling Pathway. *Marine Drugs*, 11(6):1899–1908, June 2013.
- [7] C.-T. Wang, Y.-Y. Wang, W.-S. Liu, C.-M. Cheng, K.-H. Chiu, L.-L. Liu, X.-Z. Liu, Z.-H. Wen, Y.-H. Chen, and T.-M. Chen. Rhodobacter sphaeroides Extract Lycogen™ Attenuates Testosterone-Induced Benign Prostate Hyperplasia in Rats. *International Journal of Molecular Sciences*, 19(4):1137, Apr. 2018.
- [8] K. M. Hangos and I. T. Cameron. *Process modelling and model analysis*. Academic Press, 4 edition, 2001.

- [9] D. J. Batstone. Mathematical modelling of anaerobic reactors treating domestic wastewater: Rational criteria for model use. *Reviews in Environmental Science and Biotechnology*, 5(1):57–71, 2006. ISBN: 1569-1705.
- [10] I. Takacs, G. Patry, and D. Nolasco. A dynamic model of the clarification-thickening process. *Water Research*, 25(10):1263–1271, Oct. 1991.
- [11] S. Szilvester, B. Raduly, B. Abraham, S. Lanyi, and D. R. Niculae. Mathematical Models for Domestic Biological Wastewater Treatment Process. *Environmental Engineering and Management Journal*, 9(5):629–636, 2010. ISBN: 1582-9596.
- [12] D. J. Batstone, J. Keller, and J. P. Steyer. A review of ADM1 extensions, applications, and analysis: 2002-2005. *Water Science and Technology*, 54(4):1–10, 2006. ISBN: 1843395789.
- [13] C. N. Hunter, F. Daldal, M. C. Thurnauer, and J. T. Beatty. *The Purple Phototrophic Bacteria*, volume 28. Springer, 2008. arXiv: 1011.1669v3 ISSN: 1098-6596.
- [14] T. Hülzen, D. J. Batstone, and J. Keller. Phototrophic bacteria for nutrient recovery from domestic wastewater. *Water Research*, 50:18–26, 2014.
- [15] G. C. Gordon and J. B. McKinlay. Calvin cycle mutants of photoheterotrophic purple nonsulfur bacteria fail to grow due to an electron imbalance rather than toxic metabolite accumulation. *Journal of Bacteriology*, 196(6):1231–1237, 2014.
- [16] S. Klamt, S. Schuster, and E. D. Gilles. Calculability analysis in underdetermined metabolic networks illustrated by a model of the central metabolism in purple nonsulfur bacteria. *Biotechnology and Bioengineering*, 77(7):734–751, 2002. ISBN: 0006-3592 (Print)\r0006-3592 (Linking).
- [17] R. J. Cogdell, A. Gall, and J. Köhler. The architecture and function of the light-harvesting apparatus of purple bacteria: from single molecules to in vivo membranes. *Quarterly reviews of biophysics*, 39(3):227–324, 2006. ISBN: 0033-5835 (Print).
- [18] K. J. Hellingwerf, W. Crielaard, W. D. Hoff, H. C. Matthijs, L. R. Mur, and B. J. van Rotterdam. Photobiology of bacteria. *Antonie van Leeuwenhoek*, 65(4):331–347, 1994.
- [19] D. Gaden. *Modelling anaerobic Digesters in Three Dimensions: Integration of Biochemistry with Computational Fluid Dynamics*. PhD thesis, 2013. arXiv: 1011.1669v3 ISBN: 9788578110796 ISSN: 1098-6596.
- [20] M. G. Wood, P. F. Greenfield, T. Howes, M. R. Johns, and J. Keller. Computational Fluid Dynamic Modelling of Wastewater Ponds to Improve Design. *Water Science and Technology*, 31(12):111–118, 1995.
- [21] H. K. Versteeg and W. Malalasekera. *An Introduction to Computational Fluid Dynamics: The Finite Volume Method*. Pearson Education Limited, Upper Saddle River, 2 edition, 2007.

- [22] H. Versteeg and W. Malalasekera. An Introduction to Computational Fluid Dynamics - The Finite Volume Method. *Fluid flow handbook. McGraw-Hill ...*, page 267, 1995. arXiv: 1011.1669v3 ISBN: 0-470-23515-2.
- [23] J. P. Bitog, I. B. Lee, C. G. Lee, K. S. Kim, H. S. Hwang, S. W. Hong, I. H. Seo, K. S. Kwon, and E. Mostafa. Application of computational fluid dynamics for modeling and designing photobioreactors for microalgae production: A review. *Computers and Electronics in Agriculture*, 76(2):131–147, 2011. Publisher: Elsevier B.V. ISBN: 0168-1699.
- [24] A. Lapin and A. Luebbert. Numerical simulation of the dynamics of two-phase gas-liquid flows in bubble columns. *Chemical Engineering Science*, 49(21):3661–3674, 1994. ISBN: 0009-2509.
- [25] F. Lehr, M. Millies, and D. Mewes. Bubble-size distributions and flow fields in bubble columns. *AICHE Journal*, 48(11):2426–2443, 2002. ISBN: 0001-1541.
- [26] D. Pfleger and S. Becker. Modelling and simulation of the dynamic flow behaviour in a bubble column. *Chemical Engineering Science*, 56:1737–1747, 2001. ISBN: 0009-2509.
- [27] V. V. Buwa and V. V. Ranade. Dynamics of gas-liquid flow in a rectangular bubble column : experiments and single/multi-group CFD simulations. *Chemical Engineering Science*, 57:4715–4736, 2002.
- [28] V. Pareek, S. Cox, M. Brungs, B. Young, and a. Adesina. Computational fluid dynamic (CFD) simulation of a pilot-scale annular bubble column photocatalytic reactor. *Chemical Engineering Science*, 58(3-6):859–865, 2003.
- [29] K. Ekambara, M. T. Dhotre, and J. B. Joshi. CFD simulations of bubble column reactors: 1d, 2d and 3d approach. *Chemical Engineering Science*, 60(23):6733–6746, 2005.
- [30] A. Sokolichin and G. Eigenberger. Applicability of the standard k-epsilon turbulence model to the dynamic simulation of bubble columns: Part I. Detailed numerical simulations. *Chemical Engineering Science*, 54(13-14):2273–2284, 1999.
- [31] Q. Zhang, X. Wu, S. Xue, K. Liang, and W. Cong. Study of hydrodynamic characteristics in tubular photobioreactors. *Bioprocess and Biosystems Engineering*, 36(2):143–150, 2013.
- [32] V. V. Buwa, D. S. Deo, and V. V. Ranade. Eulerian-Lagrangian simulations of unsteady gas-liquid flows in bubble columns. *International Journal of Multiphase Flow*, 32(7):864–885, 2006. ISBN: 0301-9322.
- [33] M. Göz, S. Laín, and M. Sommerfeld. Study of the numerical instabilities in Lagrangian tracking of bubbles and particles in two-phase flow. *Computers & Chemical Engineering*, 28(12):2727–2733, 2004.

- [34] H. P. Luo and M. H. Al-Dahhan. Verification and validation of CFD simulations for local flow dynamics in a draft tube airlift bioreactor. *Chemical Engineering Science*, 66(5):907–923, 2011. Publisher: Elsevier ISBN: 0009-2509.
- [35] S. Lain, D. Bröder, M. Sommerfeld, and M. Göz. Modelling hydrodynamics and turbulence in a bubble column using the Euler–Lagrange procedure. *International Journal of Multiphase Flow*, 28(8):1381–1407, 2002.
- [36] K. a. Mouza, N. a. Kazakis, and S. V. Paras. Bubble column reactor design using a CFD code. In *1st International Conference From Scientific Computing to Computational Engineering Athens*, pages 1–8, 2004.
- [37] A. Soman and Y. Shastri. Optimization of novel photobioreactor design using computational fluid dynamics. *Applied Energy*, 140:246–255, 2015. Publisher: Elsevier Ltd ISBN: 2225767203.
- [38] C. Posten. Design principles of photo-bioreactors for cultivation of microalgae. *Engineering in Life Sciences*, 9(3):165–177, 2009. ISBN: 1618-0240.
- [39] J. Bridgeman. Computational fluid dynamics modelling of sewage sludge mixing in an anaerobic digester. *Advances in Engineering Software*, 44(1):54–62, 2012. Publisher: Elsevier Ltd ISBN: 9781905088300.
- [40] P. J. Roache. Code Verification by the Method of Manufactured Solutions. *Journal of Fluids Engineering*, 124(1):4, 2002. arXiv: 1602.06747 ISBN: 0098-2202.
- [41] W. L. Oberkampf and T. G. Trucano. Verification and validation in computational fluid dynamics. *Prog. Aerosp. Sci.*, 38(3):209–272, Apr. 2002. ISBN: 1505844452.
- [42] I. B. Celik, U. Ghia, P. J. Roache, C. J. Freitas, H. Coleman, and P. E. Raad. Procedure for Estimation and Reporting of Uncertainty Due to Discretization in CFD Applications. *Journal of Fluids Engineering*, 130(7):78001, 2008. ISBN: 0098-2202.
- [43] D. Pelletier. Verification, validation, and uncertainty in computational fluids dynamics. *Canadian Journal of Civil Engineering*, 37(7):1003–1013, July 2010.
- [44] E. Wicklein, D. J. Batstone, J. Ducoste, J. Laurent, A. Griborio, J. Wicks, S. Saunders, R. Samstag, O. Potier, and I. Nopens. Good modelling practice in applying computational fluid dynamics for WWTP modelling. *Water Science and Technology*, 2016. ISBN: 0273-1223 (Print)\r0273-1223 (Linking).
- [45] F. R. Menter, M. Kuntz, and R. Langtry. Ten Years of Industrial Experience with the SST Turbulence Model. *Turbul. Heat Mass Transf.* 4, 4:625–632, 2003.
- [46] T.-H. Shih, W. W. Liou, A. Shabbir, Z. Yang, and J. Zhu. A new k- eddy viscosity model for high reynolds number turbulent flows. *Comput. Fluids*, 24(3):227–238, Mar. 1995.

- [47] F. R. Menter. Two-equation eddy-viscosity turbulence models for engineering applications. *AIAA J.*, 32(8):1598–1605, Aug. 1994.
- [48] J. d. S. Castro, M. L. Calijuri, P. P. Assemany, P. R. Cecon, I. R. de Assis, and V. J. Ribeiro. Microalgae biofilm in soil: Greenhouse gas emissions, ammonia volatilization and plant growth. *Science of The Total Environment*, 574:1640–1648, 2017.
- [49] K. Zhang and K. Farahbakhsh. Removal of native coliphages and coliform bacteria from municipal wastewater by various wastewater treatment processes: implications to water reuse. *Water research*, 41(12):2816–24, June 2007.
- [50] M. F. Modest. The Method of Discrete Ordinates (SN-Approximation). In *Radiative Heat Transfer*, pages 498–538. Elsevier, Amsterdam, 2 edition, 2003.
- [51] C.-G. Lee and B. Palsson. High-Density Algal Photobioreactors Using Light-Emitting Diodes. *Biotechnology and Bioengineering*, 44(10):1161–1167, 1994. ISBN: 0006-3592.
- [52] H. Berberoglu and L. Pilon. Experimental measurements of the radiation characteristics of Anabaena variabilis ATCC 29413-U and Rhodobacter sphaeroides ATCC 49419. *International Journal of Hydrogen Energy*, 32:4772–4785, 2007.
- [53] L. Pottier, J. Pruvost, J. Deremetz, J. F. Cornet, J. Legrand, and C. G. Dussap. A fully predictive model for one-dimensional light attenuation by Chlamydomonas reinhardtii in a torus photobioreactor. *Biotechnology and Bioengineering*, 91(5):569–582, 2005.
- [54] L.-l. Wang, Y. Tao, and X.-z. Mao. A novel flat plate algal bioreactor with horizontal baffles: Structural optimization and cultivation performance. *Bioresource Technology*, 164:20–27, 2014. Publisher: Elsevier Ltd.
- [55] J. S. Marshall and Y. Huang. Simulation of light-limited algae growth in homogeneous turbulence. *Chemical Engineering Science*, 65(12):3865–3875, 2010. Publisher: Elsevier ISBN: 00092509.
- [56] Q. Béchet, A. Shilton, and B. Guieyse. Modeling the effects of light and temperature on algae growth: State of the art and critical assessment for productivity prediction during outdoor cultivation. *Biotechnology Advances*, 31(8):1648–1663, 2013. ISBN: 0734-9750.
- [57] E. K. Nauha and V. Alopaeus. Modeling method for combining fluid dynamics and algal growth in a bubble column photobioreactor. *Chemical Engineering Journal*, 229:559–568, 2013. Publisher: Elsevier B.V. ISBN: 1385-8947.
- [58] J. S. Marshall and K. Sala. A stochastic Lagrangian approach for simulating the effect of turbulent mixing on algae growth rate in a photobioreactor. *Chemical Engineering Science*, 66(3):384–392, 2011. Publisher: Elsevier ISBN: 0009-2509.

- [59] S. Zhang, D. Müller, H. Arellano-Garcia, and G. Wozny. CFD simulation of the fluid hydrodynamics in a continuous stirred-tank reactor. *Chemical Engineering Transactions*, 32:1441–1446, 2013. ISBN: 9788895608235.
- [60] M. Hochhalter and S. P. Gent. Incorporating light and algal effects into CFD for photobioreactor design. In *ASME 2014 4th Joint US-European Fluids Engineering Division Summer Meeting*, pages 1–10, 2014. ISSN: 08888116.
- [61] P. E. Gharagozloo, J. L. Drewry, A. M. Collins, T. a. Dempster, C. Y. Choi, and S. C. James. Analysis and modeling of Nannochloropsis growth in lab, greenhouse, and raceway experiments. *Journal of Applied Phycology*, 26(6):2303–2314, 2014.
- [62] S. Park and Y. Li. Integration of biological kinetics and computational fluid dynamics to model the growth of Nannochloropsis salina in an open channel raceway. *Biotechnology and Bioengineering*, 112(5):923–933, 2015.
- [63] W. Cheng, J. Huang, and J. Chen. Computational fluid dynamics simulation of mixing characteristics and light regime in tubular photobioreactors with novel static mixers. *Journal of Chemical Technology and Biotechnology*, 91(2):327–335, 2016.
- [64] F. Krujatz, R. Illing, T. Krautwer, J. Liao, K. Heibig, K. Goy, J. Opitz, G. Cuniberti, T. Bley, and J. Weber. Light-field-characterization in a continuous hydrogen-producing photobioreactor by optical simulation and computational fluid dynamics. *Biotechnology and Bioengineering*, 9999(xxx):n/a–n/a, 2015.
- [65] I. S. Suh and S. B. Lee. A light distribution model for an internally radiating photobioreactor. *Biotechnology and Bioengineering*, 82(2):180–189, 2003. ISBN: 0006-3592.
- [66] G. McDermott, S. M. Prince, A. A. Freer, A. M. Hawthornthwaite-Lawless, M. Z. Papiz, R. J. Cogdell, and N. W. Isaacs. Crystal Structure of an Integral Membrane Light-Harvesting Complex from Photosynthetic Bacteria. *Nature*, 374(517-521), 1995.
- [67] P. J. Coelho. A comparison of spatial discretization schemes for differential solution methods of the radiative transfer equation. *Journal of Quantitative Spectroscopy and Radiative Transfer*, 109(2):189–200, 2008.
- [68] B. Kong and R. D. Vigil. Simulation of photosynthetically active radiation distribution in algal photobioreactors using a multidimensional spectral radiation model. *Bioresource technology*, 158C:141–148, 2014. Publisher: Elsevier Ltd.
- [69] P. J. Coelho. Advances in the discrete ordinates and finite volume methods for the solution of radiative heat transfer problems in participating media. *Journal of Quantitative Spectroscopy and Radiative Transfer*, 145:121–146, 2014. ISBN: 0022-4073.

- [70] P. K. Pandey, G. B. Pasternack, M. Mahbubul, M. L. Soupir, and M. S. Kaiser. A neighborhood statistics model for predicting stream pathogen indicator levels. *Environmental Monitoring and Assessment*, 187:124, 2015. ISBN: 1066101442.
- [71] Z. C. Wheaton and G. Krishnamoorthy. Modeling radiative transfer in photobioreactors for algal growth. *Computers and Electronics in Agriculture*, 87:64–73, 2012. Publisher: Elsevier B.V. ISBN: 01681699 (ISSN).
- [72] Q. Huang, T. Liu, J. Yang, L. Yao, and L. Gao. Evaluation of radiative transfer using the finite volume method in cylindrical photoreactors. *Chemical Engineering Science*, 66(17):3930–3940, 2011.
- [73] A. E. Eltayeb, O. Khalil, S. Al-Hallaj, and F. Teymour. Design and modeling of optical modules for use in the "Emerald Forest" algae photobioreactors. *Computers and Chemical Engineering*, 34(9):1323–1340, 2010.
- [74] G. Krishnamoorthy, R. Klosterman, and D. Shallbetter. A Radiative Transfer Modeling Methodology in Gas-Liquid Multiphase Flow Simulations. *Journal of Engineering*, 2014, 2014.
- [75] X. Gao, B. Kong, and R. Dennis Vigil. Comprehensive computational model for combining fluid hydrodynamics, light transport and biomass growth in a Taylor vortex algal photobioreactor: Lagrangian approach. *Bioresource Technology*, 224:523–530, 2016. Publisher: Elsevier Ltd.
- [76] H. Amini, A. Hashemisohi, L. Wang, A. Shahbazi, M. Bikdash, D. KC, and W. Yuan. Numerical and experimental investigation of hydrodynamics and light transfer in open raceway ponds at various algal cell concentrations and medium depths. *Chemical Engineering Science*, 156:11–23, 2016.
- [77] T. Li, B. Podola, and M. Melkonian. Investigating dynamic processes in a porous substrate biofilm photobioreactor - A modeling approach. *Algal Research*, 13:30–40, 2016. ISBN: 2211-9264.
- [78] C. Casado, J. Marug??n, R. Timmers, M. Mu??oz, and R. van Grieken. Comprehensive multiphysics modeling of photocatalytic processes by computational fluid dynamics based on intrinsic kinetic parameters determined in a differential photoreactor. *Chemical Engineering Journal*, 310:368–380, 2017.
- [79] E. Lee, J. Pruvost, X. He, R. Munipalli, and L. Pilon. Design tool and guidelines for outdoor photobioreactors. *Chemical Engineering Science*, 106:18–29, 2014. ISBN: 0009-2509.
- [80] J. M. Heinrich, I. Niizawa, F. A. Botta, A. R. Trombert, and H. A. Irazoqui. Analysis and Design of Photobioreactors for Microalgae Production II: Experimental Validation of a Radiation Field Simulator Based on a Monte Carlo Algorithm. *Photochemistry and Photobiology*, 88(4):952–960, July 2012. Publisher: Blackwell Publishing Ltd.

- [81] J. Pruvost, J. F. Cornet, and J. Legrand. Hydrodynamics influence on light conversion in photobioreactors: An energetically consistent analysis. *Chemical Engineering Science*, 63(14):3679–3694, 2008. ISBN: 0009-2509.
- [82] L. Pilon, H. Berberoglu, and R. Kandilian. Radiation transfer in photobiological carbon dioxide fixation and fuel production by microalgae. *Journal of Quantitative Spectroscopy and Radiative Transfer*, 112(17):2639–2660, 2011. ISBN: 0022-4073.
- [83] I. Perner-Nochta and C. Posten. Simulations of light intensity variation in photobioreactors. *Journal of Biotechnology*, 131(3):276–285, 2007. ISBN: 0168-1656 (Print)\r0168-1656 (Linking).
- [84] W. Jarosz. *Efficient Monte Carlo Methods for Light Transport in Scattering Media*. PhD Thesis, University of California, San Diego, 2008.
- [85] P. H. C. Eilers and J. C. H. Peeters. A model for the relationship between light intensity and the rate of photosynthesis in phytoplankton. *Ecological Modelling*, 42:199–215, 1988.
- [86] X. Wu and J. C. Merchuk. A model integrating fluid dynamics in photosynthesis and photoinhibition processes. *Chemical Engineering Science*, 56(11):3527–3538, 2001. ISBN: 0009-2509.
- [87] X. Wu and J. C. Merchuk. Simulation of algae growth in a bench-scale bubble column reactor. *Biotechnology and Bioengineering*, 80(2):156–168, 2002. ISBN: 0006-3592.
- [88] J. C. Merchuk and X. Wu. Modeling of photobioreactors: Application to bubble column simulation. *Journal of Applied Phycology*, 15:163–169, 2003. ISBN: 0921-8971.
- [89] J. C. Merchuk, F. Garcia-Camacho, and E. Molina-Grima. Photobioreactor design and fluid dynamics. *Chemical and Biochemical Engineering Quarterly*, 21(4):345–355, 2007. ISBN: 03529568 (ISSN).
- [90] H. Marschall, K. Hinterberger, C. Schüler, F. Habla, and O. Hinrichsen. Numerical simulation of species transfer across fluid interfaces in free-surface flows using OpenFOAM. *Chemical Engineering Science*, 78:111–127, 2012. ISBN: 00092509.
- [91] D. J. Thomson. Criteria for the selection of stochastic models of particle trajectories in turbulent flows. *Journal of Fluid Mechanics*, 180:529–556, 1987.
- [92] S. Matassa, W. Verstraete, I. Pikaar, and N. Boon. Autotrophic nitrogen assimilation and carbon capture for microbial protein production by a novel enrichment of hydrogen-oxidizing bacteria. *Water Research*, 101:137–146, 2016. Publisher: Elsevier Ltd ISBN: 0043-1354.
- [93] S. Matassa, D. J. Batstone, T. Huelsen, J. L. Schnoor, and W. Verstraete. Can direct conversion of used nitrogen to new feed and protein help feed the world? *Environmental Science & Technology*, page 150327153639000, 2015.

- [94] F. G. Acién Fernández, F. García Camacho, and Y. Chisti. Photobioreactors: light regime, mass transfer, and scaleup. *Progress in Industrial Microbiology*, 35(C):231–247, 1999. ISBN: 01681656.
- [95] A. Perez-Castro, J. Sanchez-Moreno, and M. Castilla. PhotoBioLib: a Modelica library for modeling and simulation of large-scale photobioreactors. *Computers & Chemical Engineering*, 98:12–20, 2016.
- [96] D. Puyol, E. Barry, T. Huelsen, and D. Batstone. A mechanistic model for anaerobic phototrophs in domestic wastewater applications: Photo-anaerobic model (PAnM). *Water Research*, 116:241–253, 2017. Publisher: Elsevier Ltd.
- [97] D. Santoro, F. Crapulli, A. Turolla, and M. Antonelli. Detailed modeling of oxalic acid degradation by UV-TiO<sub>2</sub> nanoparticles : Importance of light scattering and photoreactor. *Water Research*, 121:361–373, 2017. Publisher: Elsevier Ltd.
- [98] E. Kayahan, I. Eroglu, and H. Koku. Design of an outdoor stacked - tubular reactor for biological hydrogen production. *International Journal of Hydrogen Energy*, 41(42):19357–19366, 2016. Publisher: Elsevier Ltd.
- [99] H. Ali, T. A. Cheema, H. S. Yoon, Y. Do, and C. W. Park. Numerical prediction of algae cell mixing feature in raceway ponds using particle tracing methods. *Biotechnology and Bioengineering*, 112(2):297–307, 2015.
- [100] G. D. Raithby and E. H. Chui. A Finite-Volume Method for Predicting a Radian Heat Transfer in Enclosures With Participating Media. *Journal of Heat Transfer*, 112(May 1990):415, 1990. ISBN: 0022-1481.
- [101] B. Uyar, I. Eroglu, M. Yücel, U. Gündüz, and L. Türker. Effect of light intensity, wavelength and illumination protocol on hydrogen production in photobioreactors. *International Journal of Hydrogen Energy*, 32(18):4670–4677, 2007. ISBN: 0360-3199.
- [102] Q. Zhou, P. Zhang, and G. Zhang. Enhancement of cell production in photosynthetic bacteria wastewater treatment by low-strength ultrasound. *Bioresource Technology*, 161:451–454, 2014. Publisher: Elsevier Ltd.
- [103] S. Bordel, B. Guiyesse, and R. Muñoz. Mechanistic Model for the Reclamation of Industrial Wastewaters Using Algal Bacterial Photobioreactors. *Environmental science & technology*, 43(9):3200–3207, 2009.
- [104] H. Y. Lee, L. E. Erickson, and S. S. Yang. Kinetics and bioenergetics of light-limited photoautotrophic growth of *Spirulina platensis*. *Biotechnology and Bioengineering*, 29(7):832–843, 1987.

- [105] O. Bernard. Hurdles and challenges for modelling and control of microalgae for CO<sub>2</sub> mitigation and biofuel production. *Journal of Process Control*, 21(10):1378–1389, 2011. Publisher: Elsevier Ltd ISBN: 9783902661708.
- [106] J. Miyake, T. Wakayama, J. Schnackenberg, T. Arai, and Y. Asada. Simulation of the daily sunlight illumination pattern for bacterial photo-hydrogen production. *Journal of Bioscience and Bioengineering*, 88(6):659–663, 1999. ISBN: 1389-1723.
- [107] B. Podola, T. Li, and M. Melkonian. Porous Substrate Bioreactors: A Paradigm Shift in Microalgal Biotechnology? *Trends in Biotechnology*, 35(2):121–132, 2017. ISBN: 0167-7799.
- [108] H. J. Eberl, D. F. Parker, and M. C. Vanloosdrecht. A new deterministic spatio-temporal continuum model for biofilm development. *Journal of Theoretical Medicine*, 3(3):161–175, 2001.
- [109] E. Alpkvist and I. Klapper. A multidimensional multispecies continuum model for heterogeneous biofilm development. *Bulletin of Mathematical Biology*, 69(2):765–789, 2007. ISBN: 0092-8240 (Print) \r 0092-8240 (Linking).
- [110] A. Rajendran and B. Hu. Mycoalgae biofilm: Development of a novel platform technology using algae and fungal cultures. *Biotechnology for Biofuels*, 9(1):1–13, 2016. ISBN: 1306801605.
- [111] T. E. Murphy and H. Berberoglu. Flux balancing of light and nutrients in a biofilm photobioreactor for maximizing photosynthetic productivity. *Biotechnology Progress*, 30(2):348–359, 2014.

*When the spirits are low, when the day appears dark, when work becomes monotonous, when hope hardly seems worth having, just mount a bicycle and go out for a spin down the road, without thought on anything but the ride you are taking.*

Arthur Conan Doyle